Numerical Algorithms (2020) 84:133–163
https://doi.org/10.1007/s11075-019-00749-z

ORIGINAL PAPER

A finite difference approximation of reduced coupled model for slightly compressible Forchheimer fractures in Karst aquifer system

Wei Liu[1] **· Jintao Cui**[2] **· Zhifeng Wang**[3]

Received: 11 September 2018 / Accepted: 4 June 2019 / Published online: 28 June 2019
© Springer Science+Business Media, LLC, part of Springer Nature 2019

Abstract
A finite difference method is proposed for solving the compressible reduced coupled model, in which the flow is governed by Forchheimer's law in the fracture and Darcy's law in the surrounding porous media. By using the averaging technique, the fracture is reduced to a lower dimensional interface and a more complicated transmission condition is derived on the fracture-interface. Different degrees of freedom are located on both sides of fracture-interface in order to capture the jump of velocity and pressure. Second-order error estimates in discrete norms are derived on nonuniform staggered grids for both pressure and velocity. The proposed scheme can also be extended to nonmatching spatial and temporal grids without loss of accuracy. Numerical experiments are performed to demonstrate the efficiency and accuracy of the numerical method. It is shown that the parameter ξ has little influence on the fluid flow, and the permeability tensor of fracture has a significant impact on the flow rate in both the surrounding porous and fracture-interface.

Keywords Karst aquifers · Finite difference method · Reduced model · Forchheimer equation

Mathematics Subject Classifications (2010) 65M12 · 65M15 · 65M06

✉ Wei Liu
sdu_liuwei@163.com

[1] School of Mathematics and Statistics Science, Ludong University, Yantai, 264025, China

[2] Department of Applied Mathematics, The Hong Kong Polytechnic University, Kowloon, Hong Kong

[3] School of Mathematics and Information Sciences, Yantai University, Yantai, 264005, China

1 Introduction

The fractures are considered to be the storage spaces of drinkable groundwater and occurrence sites of environmental pollution in Karst aquifer system. It is important to gain a better understanding of groundwater flow in aquifer with fractures, in order to assess groundwater risk and control pollution. Due to the close connection between the fracture and surrounding medium, a coupled model is usually applied to demonstrate the groundwater flow process in fractured media aquifer system, where the flux exchange at the junction between the fracture and surrounding medium is treated as a coupling term (see [1–4] for details).

The permeability of the fracture may differ greatly from that of the surrounding medium. It has a very important influence on the flow rate in the whole domain. Under the condition that the fluid flow in the fracture is sufficiently rapid, the linear relationship between the velocity and the pressure gradient is invalid [5–8]. By adding a quadratic term in velocity, the Forchheimer equation is used to model the flow of fluid in the fracture. It indicates that a coupled model demonstrating the flow in the fractured media is quite different from Darcy's model in [9–13]. Due to the fact that the thickness of fracture is much smaller than characteristic diameters of surrounding porous medium, the fracture can be reduced into an interface of co-dimension one. The dimension reducing process can be carried out by averaging across the fracture as in [9, 12–18]. As a result, one can reduce the cost of computation without losing the physical properties of fractured media and avoid from refining locally around the fracture.

In the past, researchers have studied the reduced Darcy flow in fracture theoretically and numerically such as by finite volume method in [9, 11, 19, 20], by extended finite element method in [10], and by RT_0 mixed finite element method in [12, 13]. Recently, the Forchheimer model in the fracture starts to receive a great deal of attention. Frih et al. [21] gave the incompressible reduced model with the Darcy equation in porous medium and the Forchheimer equation in fracture. The discrete formulation was derived by using mixed finite element method and some numerical examples were presented therein. Knabner et al. [22] considered the steady model problem with the Darcy flow in the porous media and the Forchheimer flow. The existence and uniqueness of the solutions were established for the problem. However, the flow in the fracture along the direction normal to the fracture was described by Darcy's law in [22], and the pressure was assumed to be continuous across the fracture-interface in [21]. The convergence analysis was not given in both [21] and [22].

In this paper, we consider the case where the Forchheimer law governs the flow along both directions normal and tangential to the fracture. Our model problem is different from the ones in [21] and [22]. By using averaging across the fracture, a more complicated transmission condition on the fracture-interface is obtained to describe the process of flux exchange between the fracture and surrounding medium, which makes sense in practice. An additional term corresponding to the flux of surrounding medium in and out of the fracture-interface is added to the fracture-interface equation. The reduced coupled model is no longer assumed to have continuous pressure across the fracture-interface. The flow of fluid in surrounding domain is considered to obey Darcy's law. In other words, reduced coupled model will be analyzed and simulated in this paper (cf. Fig. 1).

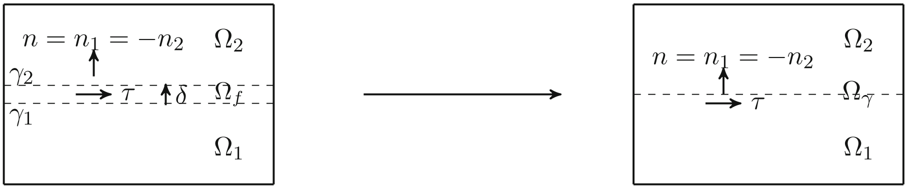

Fig. 1 The sketch figure of whole domain. Left: the convex domain is divided by the fracture region Ω_f with the thickness δ into Ω_1 and Ω_2. Right: Ω_f is treated as a fracture-interface Ω_γ between subdomains Ω_1 and Ω_2

As far as we know, there is no study of finite difference method for compressible Forchheimer fractured models with Neumann boundary condition. In this paper, we use the coupled block-centered finite difference scheme to solve the reduced coupled model. The block-centered finite difference method [23–29] is also considered as the lowest order Raviart-Thomas mixed element method with proper quadrature formulation. The application of the finite difference enables us to approximate both the velocity and pressure with second-order accuracy. Moreover, the block-centered finite difference method transfers the saddle point system of the mixed element method into a symmetric positive definite system. Based on the high-order interpolation operators, the finite difference scheme proposed in this work can be applied efficiently to solve the reduced coupled model with a complicated transmission condition. Its novelty is that degrees of freedom are introduced separately on both sides of fracture domain to capture the jump in the normal component of the velocity. When the flow moves rapidly in the fracture, smaller grids in space and time may need to be employed in fracture domain than in the surrounding medium. Such requirement brings a multi-scale challenge to the numerical methods for the reduced model. The finite difference method studied in this paper can be easily extended to solve the reduced models on nonmatching spatial and temporal grids, which is another advantage of the proposed scheme. In order to preserve accuracy of the extended methods on nonmatching grids, some properly defined interpolation operators are applied in different domains.

In the numerical experiments, second-order convergence rates are verified for the finite difference approximations of the reduced coupled model. For the fractured system, one can observe that the numerical solutions are discontinuous across the fracture-interface, and the behavior of velocity and pressure is clearly different on two sides of domain. It is also illustrated that there is little influence of the parameter ξ on the numerical solutions for the reduced coupled model. Moreover, the normal and tangential components of permeability tensor play important roles in affecting the flow rates in the surrounding porous media and fracture-interface, respectively.

The rest of the paper is organized as follows. In Section 2, the reduced coupled model is derived for the Forchheimer flow in the fracture and the Darcy flow in the surrounding porous media. In Section 3, a coupled block-centered finite difference method is introduced for the compressible reduced coupled model in fractured media aquifer system. The method is then extended to nonmatching grids for fracture and surrounding porous media in both space and time. The error analysis of the schemes is derived in Section 4. In Section 5, several numerical examples are presented to illustrate the method's accuracy and efficiency. The numerical results of some practical problems demonstrate the desired physical properties of compressible reduced coupled model. The conclusions are given in Section 6.

Throughout this paper, we use C to denote a generic positive constant independent of the discretization parameters, which may take different values in different appearances.

2 The reduced coupled model

In this section, we describe the original model and derive the reduced coupled model for the flow in the Forchheimer fractured system.

We suppose that the flow in convex domains Ω_1 and Ω_2 is governed by a mass conservation equation and the Darcy equation connecting the pressure p and velocity $\mathbf{u}$. The flow in the fracture Ω_f is governed by Forchheimer's law describing a nonlinear relationship between the velocity $\mathbf{u}_f$ and pressure p_f. For slightly compressible fluid, the density ρ_f depends on the pressure p_f, i.e., $\rho_f = \rho_f(p_f)$. Then, the original coupled model with Neumann boundary condition is given as follows,

$$\begin{cases} s_i \partial_t p_i + \mathrm{div}\mathbf{u}_i = q_i, & \text{in } \Omega_i \times J, \quad i = 1, 2, & (2.1) \\ \mathbf{u}_i = -\mathbb{K}_i \nabla p_i, & \text{in } \Omega_i \times J, \quad i = 1, 2, & (2.2) \\ \phi_f C_f^F \partial_t p_f + \mathrm{div}\mathbf{u}_f = q_f, & \text{in } \Omega_f \times J, & (2.3) \\ \mu_f \mathbf{u}_f + \mathbb{K}_f \beta_f \rho_f(p_f)|\mathbf{u}_f|\mathbf{u}_f + \mathbb{K}_f \nabla p_f = 0, & \text{in } \Omega_f \times J, & (2.4) \\ \mathbf{u}_i \cdot \mathbf{n}_i = \mathbf{u}_f \cdot \mathbf{n}_i, & \text{on } \gamma_i \times J, \quad i = 1, 2, & (2.5) \\ p_i = p_f, & \text{on } \gamma_i \times J, \quad i = 1, 2, & (2.6) \\ \mathbf{u}_i \cdot \nu_i = g_i, & \text{on } \Gamma_i \times J, \quad i = 1, 2, f, & (2.7) \\ p_i(\cdot, 0) = p_i^0, & \text{in } \Omega_i, \quad i = 1, 2, f, & (2.8) \end{cases}$$

where the time interval $J = (0, T]$. s is the storage coefficient, $\mathbb{K}$ is the permeability tensor (or hydraulic conductivity), q is the source or sink term, $g \in L^2(\partial\Omega)$ is the given flux through the boundary, p^0 are the given pressure on the initial time level, respectively. Let $p|_{\Omega_i} = p_i, \mathbf{u}|_{\Omega_i} = \mathbf{u}_i, s|_{\Omega_i} = s_i, \mathbb{K}|_{\Omega_i} = \mathbb{K}_i, g|_{\Omega_i} = g_i, q|_{\Omega_i} = q_i, p|^0_{\Omega_i} = p_i^0$, Γ_i is the boundary of Ω_i, ν_i is unit outer normal vector to Ω_i $(i = 1, 2, f)$. Here, we assume that $\mathbb{K}_i = \begin{pmatrix} K_i^x & 0 \\ 0 & K_i^y \end{pmatrix}$, and there exist positive constants κ_i^x and κ_i^y for $i = 1, 2, f$ such that

$$\kappa_1^x \le K_i^x \le \kappa_2^x, \qquad \kappa_1^y \le K_i^y \le \kappa_2^y.$$

The notation $|\cdot|$ represents the Euclidean norm, i.e., $|\mathbf{u}_f|^2 = \mathbf{u}_f \cdot \mathbf{u}_f$. The constant μ_f denotes the viscosity coefficient of the fluid in fracture; the constant β_f denotes the Forchheimer number; the constant ϕ_f is the porosity and C_f^F is the coefficient of compressibility. The parameters of Forchheimer equation in fracture are assumed to be constants.

Next, we use the technique of averaging across the fracture in order to reduce the model to be one-dimensional.

For the conservation (2.3) in the fracture, we have the following equations such as in [12]

$$\mathrm{div}_\tau u_\gamma = q_\gamma + (\mathbf{u}_1 \cdot \mathbf{n}_1|_{\Omega_\gamma} + \mathbf{u}_2 \cdot \mathbf{n}_2|_{\Omega_\gamma}), \qquad \text{on } \Omega_\gamma, \tag{2.9}$$

by using (2.5). Here, div_τ denotes the tangential divergence, $u_\gamma = \int_{-\frac{\delta}{2}}^{\frac{\delta}{2}} u_f^\tau dn$ and $q_\gamma = \int_{-\frac{\delta}{2}}^{\frac{\delta}{2}} q_f dn$.

Equation (2.9) models the mass conservation equation inside fracture-interface Ω_γ. A source term $(\mathbf{u}_1 \cdot \mathbf{n}_1|_{\Omega_\gamma} + \mathbf{u}_2 \cdot \mathbf{n}_2|_{\Omega_\gamma})$ is introduced to characterize the difference between the flow in and out of the fracture.

For the Forchheimer equation (2.4), we divide it into two parts according to the tangential and normal directions as follows,

$$\mu_f u_f^\tau + K_f^\tau \beta_f \rho_f(p_f)|\mathbf{u}_f|u_f^\tau + K_f^\tau \nabla_\tau p_f = 0, \tag{2.10}$$

$$\mu_f u_f^n + K_f^n \beta_f \rho_f(p_f)|\mathbf{u}_f|u_f^n + K_f^n \nabla_n p_f = 0. \tag{2.11}$$

where ∇_τ denotes the tangential gradient. Note that our equation (2.11) is different from (9b) in [21] and (13) in [22], in which the flow in the fracture along normal direction satisfies Darcy's law.

By using the constant assumption of the parameters in Forchheimer equations and integrating both sides of (2.10) on the section $(-\frac{\delta}{2}, \frac{\delta}{2})$, we get

$$\mu_\gamma \int_{-\frac{\delta}{2}}^{\frac{\delta}{2}} u_f^\tau dn + K_\gamma^\tau \beta_\gamma \int_{-\frac{\delta}{2}}^{\frac{\delta}{2}} \rho_f(p_f)|\mathbf{u}_f|u_f^\tau dn + K_\gamma^\tau \nabla_\tau \int_{-\frac{\delta}{2}}^{\frac{\delta}{2}} p_f dn = 0. \tag{2.12}$$

Under the condition that the thickness of fracture δ is very small and $\delta u_f^\tau \approx u_\gamma$, we have

$$|\mathbf{u}_f| = \sqrt{(u_f^\tau)^2 + (u_f^n)^2} \approx \sqrt{(\frac{u_\gamma}{\delta})^2 + (\frac{u_f \cdot n|_{\gamma_1} + u_f \cdot n|_{\gamma_2}}{2})^2} \approx \frac{1}{\delta}|u_\gamma|. \tag{2.13}$$

Note that $\rho_f(p_f) = \rho_f^0 e^{C_f^F(p_f - p_f^0)} \approx \rho_f^0(1 + C_f^F(p_f - p_f^0))$, then $\rho_f(p_f)$ can be approximated as a linear function of p_f. We can then apply rectangle quadrature formula and (2.13) to (2.12) and obtain

$$\mu_\gamma u_\gamma + \frac{K_\gamma^\tau \beta_\gamma \rho_\gamma(p_\gamma)}{\delta}|u_\gamma|u_\gamma + K_\gamma^\tau \delta \nabla_\tau p_\gamma = 0. \tag{2.14}$$

Here $p_\gamma = \frac{1}{\delta}\int_{-\frac{\delta}{2}}^{\frac{\delta}{2}} p_f dn$, which represents the average pressure along the normal direction cross the fracture. Equation (2.14) describes Forchheimer's law in the direction tangential to the fracture-interface Ω_γ.

In order to derive the interior boundary condition on Ω_γ, we use three different approaches to cope with (2.11).

(I). By integrating both sides of (2.11) across the fracture over interval $(-\frac{\delta}{2}, \frac{\delta}{2})$, we have

$$\mu_\gamma \int_{-\frac{\delta}{2}}^{\frac{\delta}{2}} u_f^n dn + K_\gamma^n \beta_\gamma \int_{-\frac{\delta}{2}}^{\frac{\delta}{2}} \rho_f(p_f)|\mathbf{u}_f|\, u_f^n dn + K_\gamma^n (p_2|_{\Omega_\gamma} - p_1|_{\Omega_\gamma}) = 0, \quad (2.15)$$

which is obtained by the pressure relationship (2.6).

By trapezoidal integral formula, (2.5) and (2.13), we get

$$\mu_\gamma \frac{\delta}{2}(\mathbf{u}_f \cdot \mathbf{n}|_{\gamma_1} + \mathbf{u}_f \cdot \mathbf{n}|_{\gamma_2}) + K_\gamma^n \beta_\gamma \rho_\gamma(p_\gamma)|u_\gamma| \frac{(\mathbf{u}_f \cdot \mathbf{n}|_{\gamma_1} + \mathbf{u}_f \cdot \mathbf{n}|_{\gamma_2})}{2}$$
$$+ K_\gamma^n (p_2|_{\Omega_\gamma} - p_1|_{\Omega_\gamma}) = 0. \quad (2.16)$$

Setting $\alpha_\gamma = 2K_\gamma^n/\delta$ and using (2), we arrive at

$$\mu_\gamma(\mathbf{u}_1 \cdot \mathbf{n}_1|_{\Omega_\gamma} - \mathbf{u}_2 \cdot \mathbf{n}_2|_{\Omega_\gamma}) + \frac{\alpha_\gamma \beta_\gamma \rho_\gamma(p_\gamma)|u_\gamma|}{2}(\mathbf{u}_1 \cdot \mathbf{n}_1|_{\Omega_\gamma} - \mathbf{u}_2 \cdot \mathbf{n}_2|_{\Omega_\gamma})$$
$$+ \alpha_\gamma(p_2|_{\Omega_\gamma} - p_1|_{\Omega_\gamma}) = 0. \quad (2.17)$$

Together with $p_\gamma \approx \frac{p_2|_{\Omega_\gamma} + p_1|_{\Omega_\gamma}}{2}$, we obtain

$$-\frac{1}{2}(\mu_\gamma + \frac{\alpha_\gamma \beta_\gamma \rho_\gamma(p_\gamma)|u_\gamma|}{2}) \quad \mathbf{u}_1 \cdot \mathbf{n}_1|_{\Omega_\gamma} + \alpha_\gamma p_1|_{\Omega_\gamma}$$
$$= -\frac{1}{2}(\mu_\gamma + \frac{\alpha_\gamma \beta_\gamma \rho_\gamma(p_\gamma)|u_\gamma|}{2})\mathbf{u}_2 \cdot \mathbf{n}_2|_{\Omega_\gamma} + \alpha_\gamma p_\gamma, \quad (2.18)$$
$$-\frac{1}{2}(\mu_\gamma + \frac{\alpha_\gamma \beta_\gamma \rho_\gamma(p_\gamma)|u_\gamma|}{2}) \quad \mathbf{u}_2 \cdot \mathbf{n}_2|_{\Omega_\gamma} + \alpha_\gamma p_2|_{\Omega_\gamma}$$
$$= -\frac{1}{2}(\mu_\gamma + \frac{\alpha_\gamma \beta_\gamma \rho_\gamma(p_\gamma)|u_\gamma|}{2})\mathbf{u}_1 \cdot \mathbf{n}_1|_{\Omega_\gamma} + \alpha_\gamma p_\gamma. \quad (2.19)$$

(II). By integrating (2.11) on interval $(-\frac{\delta}{2}, 0)$ and $(0, \frac{\delta}{2})$, respectively, we get

$$\mu_\gamma \int_{-\frac{\delta}{2}}^{0} u_f^n dn + K_\gamma^n \beta_\gamma \int_{-\frac{\delta}{2}}^{0} \rho_f(p_f)|\mathbf{u}_f| u_f^n dn + K_\gamma^n \int_{-\frac{\delta}{2}}^{0} \nabla_n p_f dn = 0, \quad (2.20)$$
$$\mu_\gamma \int_{0}^{\frac{\delta}{2}} u_f^n dn + K_\gamma^n \beta_\gamma \int_{0}^{\frac{\delta}{2}} \rho_f(p_f)|\mathbf{u}_f| u_f^n dn + K_\gamma^n \int_{0}^{\frac{\delta}{2}} \nabla_n p_f dn = 0. \quad (2.21)$$

By trapezoidal integral formula,

$$-\frac{3}{4}(\mu_\gamma + \frac{\alpha_\gamma \beta_\gamma \rho_\gamma(p_\gamma)|u_\gamma|}{2}) \quad \mathbf{u}_1 \cdot \mathbf{n}_1|_{\Omega_\gamma} + \alpha_\gamma p_1|_{\Omega_\gamma}$$
$$= -\frac{1}{4}(\mu_\gamma + \frac{\alpha_\gamma \beta_\gamma \rho_\gamma(p_\gamma)|u_\gamma|}{2})\mathbf{u}_2 \cdot \mathbf{n}_2|_{\Omega_\gamma} + \alpha_\gamma p_\gamma, \quad (2.22)$$
$$-\frac{3}{4}(\mu_\gamma + \frac{\alpha_\gamma \beta_\gamma \rho_\gamma(p_\gamma)|u_\gamma|}{2}) \quad \mathbf{u}_2 \cdot \mathbf{n}_2|_{\Omega_\gamma} + \alpha_\gamma p_2|_{\Omega_\gamma}$$
$$= -\frac{1}{4}(\mu_\gamma + \frac{\alpha_\gamma \beta_\gamma \rho_\gamma(p_\gamma)|u_\gamma|}{2})\mathbf{u}_1 \cdot \mathbf{n}_1|_{\Omega_\gamma} + \alpha_\gamma p_\gamma. \quad (2.23)$$

(III). By using rectangular integrate formula to (2.20) and (2.21), we obtain

$$(\mu_\gamma + \frac{\alpha_\gamma \beta_\gamma \rho_\gamma(p_\gamma)|u_\gamma|}{2})\mathbf{u}_1 \cdot \mathbf{n}_1|_{\Omega_\gamma} - K_\gamma^n \frac{p_1|_{\Omega_\gamma} - p_\gamma}{\delta/2} = 0, \tag{2.24}$$

$$(\mu_\gamma + \frac{\alpha_\gamma \beta_\gamma \rho_\gamma(p_\gamma)|u_\gamma|}{2})\mathbf{u}_2 \cdot \mathbf{n}_2|_{\Omega_\gamma} - K_\gamma^n \frac{p_2|_{\Omega_\gamma} - p_\gamma}{\delta/2} = 0. \tag{2.25}$$

Then,

$$-(\mu_\gamma + \frac{\alpha_\gamma \beta_\gamma \rho_\gamma(p_\gamma)|u_\gamma|}{2})\mathbf{u}_1 \cdot \mathbf{n}_1|_{\Omega_\gamma} + \alpha_\gamma p_1|_{\gamma_1} = \alpha_\gamma p_\gamma, \tag{2.26}$$

$$-(\mu_\gamma + \frac{\alpha_\gamma \beta_\gamma \rho_\gamma(p_\gamma)|u_\gamma|}{2})\mathbf{u}_2 \cdot \mathbf{n}_2|_{\Omega_\gamma} + \alpha_\gamma p_2|_{\gamma_2} = \alpha_\gamma p_\gamma. \tag{2.27}$$

Combining the above three cases, we have the following general transmission condition on the fracture-interface,

$$\begin{aligned} -\xi(\mu_\gamma + \frac{\alpha_\gamma \beta_\gamma \rho_f(p_\gamma)|u_\gamma|}{2}) &\quad \mathbf{u}_1 \cdot \mathbf{n}_1|_{\Omega_\gamma} + \alpha_\gamma p_1|_{\Omega_\gamma} \\ &= -(1-\xi)(\mu_\gamma + \frac{\alpha_\gamma \beta_\gamma \rho_\gamma(p_\gamma)|u_\gamma|}{2})\mathbf{u}_2 \cdot \mathbf{n}_2|_{\Omega_\gamma} + \alpha_\gamma p_\gamma, \quad (2.28) \\ -\xi(\mu_\gamma + \frac{\alpha_\gamma \beta_\gamma \rho_\gamma(p_\gamma)|u_\gamma|}{2}) &\quad \mathbf{u}_2 \cdot \mathbf{n}_2|_{\Omega_\gamma} + \alpha_\gamma p_2|_{\Omega_\gamma} \\ &= -(1-\xi)(\mu_\gamma + \frac{\alpha_\gamma \beta_\gamma \rho_\gamma(p_\gamma)|u_\gamma|}{2})\mathbf{u}_1 \cdot \mathbf{n}_1|_{\Omega_\gamma} + \alpha_\gamma p_\gamma, \quad (2.29) \end{aligned}$$

where $\xi = 1/2, \xi = 3/4, \xi = 1$. For the purpose of general applications, we take the range of parameter ξ from 1/2 to 1, i.e., $\xi \in (1/2, 1]$.

Combining the conservation equation (2.9), Forchheimer equation (2.14), and fracture-interface condition (2.28)–(2.29), we obtain the reduced coupled model as follows,

$$\begin{cases} s_i \partial_t p_i + \mathrm{div}\mathbf{u}_i = q_i, & \text{in } \Omega_i \times J, \quad i = 1, 2, \quad (2.30) \\ \mathbf{u}_i = -\mathbb{K}_i \nabla p_i, & \text{in } \Omega_i \times J, \quad i = 1, 2, \quad (2.31) \\ \phi_\gamma C_\gamma^F \partial_t p_\gamma + \mathrm{div}_\tau u_\gamma = q_\gamma + (\mathbf{u}_1 \cdot \mathbf{n}_1|_{\Omega_\gamma} + \mathbf{u}_2 \cdot \mathbf{n}_2|_{\Omega_\gamma}), & \text{on } \Omega_\gamma \times J, \quad (2.32) \\ \mu_\gamma u_\gamma + \frac{K_\gamma^\tau \beta_\gamma \rho_\gamma(p_\gamma)}{\delta}|u_\gamma| u_\gamma + K_\gamma^\tau \delta \nabla_\tau p_\gamma = 0, & \text{on } \Omega_\gamma \times J, \quad (2.33) \\ -\xi(\mu_\gamma + \frac{\alpha_\gamma \beta_\gamma \rho_\gamma(p_\gamma)|u_\gamma|}{2})\mathbf{u}_1 \cdot \mathbf{n}_1|_{\Omega_\gamma} + \alpha_\gamma p_1|_{\Omega_\gamma} & \\ \quad = -(1-\xi)(\mu_\gamma + \frac{\alpha_\gamma \beta_\gamma \rho_\gamma(p_\gamma)|u_\gamma|}{2})\mathbf{u}_2 \cdot \mathbf{n}_2|_{\Omega_\gamma} + \alpha_\gamma p_\gamma, & \text{on } \Omega_\gamma \times J, \quad (2.34) \\ -\xi(\mu_\gamma + \frac{\alpha_\gamma \beta_\gamma \rho_\gamma(p_\gamma)|u_\gamma|}{2})\mathbf{u}_2 \cdot \mathbf{n}_2|_{\Omega_\gamma} + \alpha_\gamma p_2|_{\Omega_\gamma} & \\ \quad = -(1-\xi)(\mu_\gamma + \frac{\alpha_\gamma \beta_\gamma \rho_\gamma(p_\gamma)|u_\gamma|}{2})\mathbf{u}_1 \cdot \mathbf{n}_1|_{\Omega_\gamma} + \alpha_\gamma p_\gamma, & \text{on } \Omega_\gamma \times J, \quad (2.35) \\ \mathbf{u}_i \cdot \nu_i = g_i, & \text{on } \Gamma \times J, \quad i = 1, 2, \gamma, \quad (2.36) \\ p_i(\cdot, 0) = p_i^0, & \text{in } \Omega_i, \quad i = 1, 2, \gamma. \quad (2.37) \end{cases}$$

Equation (2.32) describes the mass conservation on fracture-interface Ω_γ with an additional source term $(\mathbf{u}_1 \cdot \mathbf{n}_1|_{\Omega_\gamma} + \mathbf{u}_2 \cdot \mathbf{n}_2|_{\Omega_\gamma})$. This extra source term corresponds to the contribution of the surrounding porous media flows into the fracture-interface. Equation (2.33) is Forchheimer's law on one-dimensional fracture-interface Ω_γ. The transmission conditions (2.4)–(2.35) denote the coupling relationship between the fracture-interface Ω_γ and surrounding subdomains Ω_1, Ω_2. The exchanging flux for Forchheimer flow depends on the difference of the pressure in the fracture-interface and surrounding medium, which makes sense from the practical application point of view. Based on the assumption that the flow in fracture obeys Forchheimer's law along both normal and tangential directions of the fracture-interface, the conditions (2.4)–(2.35) are different from (9b) in [21] and (13) in [22]. It is obvious that the pressure is no longer continuous across the fracture-interface. The influence of parameter ξ on the numerical solutions will be shown in Section 5. The roles of parameters K_γ^τ and K_γ^n on the fluid flow in the fractured media will also be illustrated for a fixed fracture thickness.

3 A coupled finite difference method

In this section, we design a block-centered finite difference method to solve (2.30)–(2.37) on matching grids in Section 3.1 and nonmatching grids in Section 3.2.

3.1 Coupled scheme on matching grids

Let the two-dimensional porous media $\Omega_1 = [x_a, x_b] \times [y_a, y_c)$, $\Omega_2 = [x_a, x_b] \times (y_c, y_b]$ and one-dimensional fracture-interface $\Omega_\gamma = [x_a, x_b] \times \{y = y_c\}$. The regular space partitions $\Omega_{1h} = \Theta^x \times \Theta_1^y$, $\Omega_{2h} = \Theta^x \times \Theta_2^y$ and $\Omega_{\gamma h} = \Theta^x$ for the domains Ω_1, Ω_2 and Ω_γ are given as follows.

$$
\begin{aligned}
&\Theta^x : x_a = x_{1/2} < x_{3/2} < \cdots < x_{N_x-1/2} < x_{N_x+1/2} = x_b,\\
&\Theta_1^y : y_a = y_{1/2} < y_{3/2} < \cdots < y_{\widetilde{N}_y-1/2} < y_{\widetilde{N}_y+1/2} = y_c,\\
&\Theta_2^y : y_c = y_{\widetilde{N}_y+1/2} < y_{\widetilde{N}_y+3/2} < \cdots < y_{N_y-1/2} < y_{N_y+1/2} = y_b.
\end{aligned}
$$

Set $0 = t^0 < t^1 < \cdots < t^{N_t} = T$ and define

$$
\begin{aligned}
&\Delta t^k = t^k - t^{k-1}, && \Delta t = \max_k \{\Delta t^k\},\\
&x_m = \frac{x_{m-1/2} + x_{m+1/2}}{2}, && y_n = \frac{y_{n-1/2} + y_{n+1/2}}{2},\\
&h_m^x = x_{m+1/2} - x_{m-1/2}, && h_n^y = y_{n+1/2} - y_{n-1/2},\\
&h_{m+1/2}^x = \frac{h_{m+1}^x + h_m^x}{2} = x_{m+1} - x_m, && h_{n+1/2}^y = \frac{h_{n+1}^y + h_n^y}{2} = y_{n+1} - y_n,\\
&h_x = \max_m \{h_{m+1/2}^x, h_m^x\}, && h_y = \max_n \{h_{n+1/2}^y, h_n^y\},
\end{aligned}
$$

where $m = 1, \cdots, N_x - 1$, $n = 1, \cdots, N_y - 1$, $k = 1, \cdots, N_t$.

For $\varphi_{s,l}^k = \varphi(x_s, y_l, t^k)$ at a node-point (x_s, y_l, t^k), denote

$$[d_t\varphi]_{m,n}^k = \frac{\varphi_{m,n}^k - \varphi_{m,n}^{k-1}}{\triangle t^k},$$
$$[d_x\varphi]_{m+1/2,n}^k = \frac{\varphi_{m+1,n}^k - \varphi_{m,n}^k}{h_{m+1/2}^x}, \qquad [D_x\varphi]_{m,n}^k = \frac{\varphi_{m+1/2,n}^k - \varphi_{m-1/2,n}^k}{h_m^x},$$
$$[d_y\varphi]_{m,n+1/2}^k = \frac{\varphi_{m,n+1}^k - \varphi_{m,n}^k}{h_{n+1/2}^y}, \qquad [D_y\varphi]_{m,n}^k = \frac{\varphi_{m,n+1/2}^k - \varphi_{m,n-1/2}^k}{h_n^y}.$$

Denote

$$\Omega_{\gamma,m+1/2,\widetilde{N}_y+1/2} = (x_m, x_{m+1}) \times y_{\widetilde{N}_y+1/2},$$
$$\text{with } 1 \le m \le N_x - 1,$$
$$\Omega_{\gamma,m,\widetilde{N}_y+1/2} = (x_{m-1/2}, x_{m+1/2}) \times y_{\widetilde{N}_y+1/2},$$
$$\text{with } 1 \le m \le N_x,$$
$$\Omega_{i,m,n} = (x_{m-1/2}, x_{m+1/2}) \times (y_{n-1/2}, y_{n+1/2}),$$
$$\text{with } 1 \le m \le N_x,\ 1 \le n \le \widetilde{N}_y \text{ for } i = 1; \quad 1 \le m \le N_x,\ \widetilde{N}_y + 1 \le n \le N_y \text{ for } i = 2,$$
$$\Omega_{i,m+1/2,n} = (x_m, x_{m+1}) \times (y_{n-1/2}, y_{n+1/2}),$$
$$\text{with } 1 \le m \le N_x - 1,\ 1 \le n \le \widetilde{N}_y \text{ for } i = 1; \quad 1 \le m \le N_x - 1,\ \widetilde{N}_y + 1 \le n \le N_y \text{ for } i = 2,$$
$$\Omega_{i,m,n+1/2} = (x_{m-1/2}, x_{m+1/2}) \times (y_n, y_{n+1}),$$
$$\text{with } 1 \le m \le N_x,\ 1 \le n \le \widetilde{N}_y - 1 \text{ for } i = 1; \quad 1 \le m \le N_x,\ \widetilde{N}_y + 1 \le n \le N_y \text{ for } i = 2,$$
$$\text{Note that } n \ne \widetilde{N}_y \text{ for } \Omega_{i,m,n+1/2}.$$

For discrete functions φ and θ, define the midpoint quadrature formula on different domains such as

$$\begin{aligned}
&(\varphi_i, \theta_i)_{M,\Omega_{i,m,n}} = h_m^x h_n^y \varphi_{i,m,n}\theta_{i,m,n},\\
&(\varphi_i, \theta_i)_{X,\Omega_{i,m+1/2,n}} = h_{m+1/2}^x h_n^y \varphi_{i,m+1/2,n}\theta_{i,m+1/2,n},\\
&(\varphi_i, \theta_i)_{Y,\Omega_{i,m,n+1/2}} = h_m^x h_{n+1/2}^y \varphi_{i,m,n+1/2}\theta_{i,m,n+1/2},\\
&(\varphi_\gamma, \theta_\gamma)_{\gamma M,\Omega_{\gamma,m+1/2,\widetilde{N}_y+1/2}} = h_m^x \varphi_{\gamma,m,\widetilde{N}_y+1/2}\theta_{\gamma,m,\widetilde{N}_y+1/2},\\
&(\varphi_\gamma, \theta_\gamma)_{\gamma X,\Omega_{\gamma,m,\widetilde{N}_y+1/2}} = h_{m+1/2}^x \varphi_{\gamma,m+1/2,\widetilde{N}_y+1/2}\theta_{\gamma,m+1/2,\widetilde{N}_y+1/2}.
\end{aligned} \tag{3.1}$$

Next, we give the following definitions of the discrete inner products and semi-norms based on the above quadrature formula

$$(\varphi_1, \theta_1)_M = \sum_{m,n} (\varphi_1, \theta_1)_{M,\Omega_{1,m,n}} = \sum_{m=1}^{N_x} \sum_{n=1}^{\widetilde{N}_y} h_m^x h_n^y \varphi_{1,m,n}\theta_{1,m,n},$$
$$(\varphi_2, \theta_2)_M = \sum_{m,n} (\varphi_2, \theta_2)_{M,\Omega_{2,m,n}} = \sum_{m=1}^{N_x} \sum_{n=\widetilde{N}_y+1}^{N_y} h_m^x h_n^y \varphi_{2,m,n}\theta_{2,m,n},$$

$$
\begin{aligned}
(\varphi_1,\theta_1)_X &= \sum_{m,n}(\varphi_1,\theta_1)_{X,\Omega_{1,m+1/2,n}} = \sum_{m=1}^{N_x-1}\sum_{n=1}^{\widetilde{N}_y} h^x_{m+1/2}h^y_n\varphi_{1,m+1/2,n}\theta_{1,m+1/2,n},\\
(\varphi_2,\theta_2)_X &= \sum_{m,n}(\varphi_2,\theta_2)_{X,\Omega_{2,m+1/2,n}} = \sum_{m=1}^{N_x-1}\sum_{n=\widetilde{N}_y+1}^{N_y} h^x_{m+1/2}h^y_n\varphi_{2,m+1/2,n}\theta_{2,m+1/2,n},\\
(\varphi_1,\theta_1)_Y &= \sum_{m,n}(\varphi_1,\theta_1)_{Y,\Omega_{1,m,n+1/2}} = \sum_{m=1}^{N_x}\sum_{n=1}^{\widetilde{N}_y} h^x_m h^y_{n+1/2}\varphi_{1,m,n+1/2}\theta_{1,m,n+1/2},\\
(\varphi_2,\theta_2)_Y &= \sum_{m,n}(\varphi_2,\theta_2)_{Y,\Omega_{2,m,n+1/2}} = \sum_{m=1}^{N_x}\sum_{n=\widetilde{N}_y}^{N_y-1} h^x_m h^y_{n+1/2}\varphi_{2,m,n+1/2}\theta_{2,m,n+1/2},\\
(\varphi_\gamma,\theta_\gamma)_{\gamma M} &= \sum_{m}(\varphi_\gamma,\theta_\gamma)_{\gamma M,\Omega_{\gamma,m+1/2,\widetilde{N}_y+1/2}} = \sum_{m=1}^{N_x} h^x_m\varphi_{\gamma,m,\widetilde{N}_y+1/2}\theta_{\gamma,m,\widetilde{N}_y+1/2},\\
(\varphi_\gamma,\theta_\gamma)_{\gamma X} &= \sum_{m}(\varphi_\gamma,\theta_\gamma)_{\gamma X,\Omega_{\gamma,m,\widetilde{N}_y+1/2}} = \sum_{m=1}^{N_x-1} h^x_{m+1/2}\varphi_{\gamma,m+1/2,\widetilde{N}_y+1/2}\theta_{\gamma,m+1/2,\widetilde{N}_y+1/2},\\
\|\varphi\|^2_M &= \sum_{i=1}^{2}(\varphi_i,\varphi_i)_M,\qquad \|\varphi\|^2_X = \sum_{i=1}^{2}(\varphi_i,\varphi_i)_X,\qquad \|\varphi\|^2_Y = \sum_{i=1}^{2}(\varphi_i,\varphi_i)_Y,\\
\|\varphi\|^2_{XY} &= \|\varphi\|^2_X + \|\varphi\|^2_Y,\qquad \|\varphi\|^2_{\gamma M} = (\varphi_\gamma,\varphi_\gamma)_{\gamma M},\qquad \|\varphi\|^2_{\gamma X} = (\varphi_\gamma,\varphi_\gamma)_{\gamma X}.
\end{aligned}
$$

The freedom of pressure p is defined on the center of element. In order to get the pressure approximation of the porous media on the fracture-interface, we use the extrapolation operators I_1^p in Ω_1 and I_2^p in Ω_2, respectively, such that

$$
I_1^p\varphi_{1,m,\widetilde{N}_y+1/2} = \frac{2h^y_{\widetilde{N}_y}+h^y_{\widetilde{N}_y-1}}{h^y_{\widetilde{N}_y}+h^y_{\widetilde{N}_y-1}}\varphi_{1,m,\widetilde{N}_y} - \frac{h^y_{\widetilde{N}_y}}{h^y_{\widetilde{N}_y}+h^y_{\widetilde{N}_y-1}}\varphi_{1,m,\widetilde{N}_y-1}, \tag{3.2}
$$

$$
I_2^p\varphi_{2,m,\widetilde{N}_y+1/2} = \frac{2h^y_{\widetilde{N}_y+1}+h^y_{\widetilde{N}_y+2}}{h^y_{\widetilde{N}_y+1}+h^y_{\widetilde{N}_y+2}}\varphi_{2,m,\widetilde{N}_y+1} - \frac{h^y_{\widetilde{N}_y+1}}{h^y_{\widetilde{N}_y+1}+h^y_{\widetilde{N}_y+2}}\varphi_{2,m,\widetilde{N}_y+2}. \tag{3.3}
$$

Set

$$
|\widehat{U}|^k_{\gamma,m,\widetilde{N}_y+1/2} = \frac{|U^k_{\gamma,m+1/2,\widetilde{N}_y+1/2}| + |U^k_{\gamma,m-1/2,\widetilde{N}_y+1/2}|}{2}, \tag{3.4}
$$

$$
\overline{P}_{\gamma,m+1/2,\widetilde{N}_y+1/2} = \frac{1}{2h^x_{m+1/2}}(h^x_{m+1}P_{\gamma,m,\widetilde{N}_y+1/2} + h^x_m P_{\gamma,m+1,\widetilde{N}_y+1/2}), \tag{3.5}
$$

and

$$
a^x_\gamma(p_\gamma) = \frac{K^x_\gamma\beta_\gamma\rho_\gamma(p_\gamma)}{\delta},\ b_\gamma(p_\gamma) = \frac{\alpha_\gamma\beta_\gamma\rho_\gamma(p_\gamma)}{2}.
$$

The block-centered finite difference scheme with a backward difference in time is given to approximate $u^x_i(x_{m+1/2},y_n,t^k)$, $u^y_i(x_m,y_{n+1/2},t^k)$, $p_i(x_m,y_n,t^k)$ $(i =$

1, 2), $u_\gamma(x_{m+1/2}, y_c, t^k)$ and $p_\gamma(x_m, y_c, t^k)$ by $U^{x,k}_{i,m+1/2,n}$, $U^{y,k}_{i,m,n+1/2}$, $P^k_{i,m,n}$ (i = 1, 2), $U^k_{\gamma,m+1/2,\widetilde{N}_y+1/2}$ and $P^k_{\gamma,m,\widetilde{N}_y+1/2}$ as follows:

$$s_i[d_tP_i]^k_{m,n} + [D_xU^x_i]^k_{m,n} + [D_yU^y_i]^k_{m,n} = q^k_{i,m,n}, \tag{3.6}$$

$$U^{x,k}_{i,m+1/2,n} + K^x_i[d_xP_i]^k_{m+1/2,n} = 0, \tag{3.7}$$

$$U^{y,k}_{i,m,n+1/2} + K^y_i[d_yP_i]^k_{m,n+1/2} = 0, \tag{3.8}$$

$$\phi_\gamma C^F_\gamma[d_tP_\gamma]^k_{m,\widetilde{N}_y+1/2} + [D_xU_\gamma]^k_{m,\widetilde{N}_y+1/2} = q^k_{\gamma,m,\widetilde{N}_y+1/2} + U^{y,k}_{1,m,\widetilde{N}_y+1/2} - U^{y,k}_{2,m,\widetilde{N}_y+1/2}, \tag{3.9}$$

$$(\mu_\gamma + a^x_\gamma(\overline{P}_\gamma)|U_\gamma|^k_{m+1/2,\widetilde{N}_y+1/2})U^k_{\gamma,m+1/2,\widetilde{N}_y+1/2} + K^x_\gamma\delta[d_xP_\gamma]^k_{m+1/2,\widetilde{N}_y+1/2} = 0, \tag{3.10}$$

$$\begin{aligned}&(\mu_\gamma + b_\gamma(P_\gamma)|\widehat{U}_\gamma|^k_{\gamma,m,\widetilde{N}_y+1/2})(U^{y,k}_{1,m,\widetilde{N}_y+1/2} - U^{y,k}_{2,m,\widetilde{N}_y+1/2})\\ &\quad= \frac{\alpha_\gamma}{2\xi-1}(I_1P^k_{1,m,\widetilde{N}_y+1/2} + I_2P^k_{2,m,\widetilde{N}_y+1/2} - 2P^k_{\gamma,m,\widetilde{N}_y+1/2}),\end{aligned} \tag{3.11}$$

$$\begin{aligned}&(\mu_\gamma + b_\gamma(P_\gamma)|\widehat{U}_\gamma|^k_{\gamma,m,\widetilde{N}_y+1/2})(U^{y,k}_{1,m,\widetilde{N}_y+1/2} + U^{y,k}_{2,m,\widetilde{N}_y+1/2})\\ &\quad= \alpha_\gamma(I_1P^k_{1,m,\widetilde{N}_y+1/2} - I_2P^k_{2,m,\widetilde{N}_y+1/2}),\end{aligned} \tag{3.12}$$

$$U^{x,k}_{i,1/2,n} = -g_i(x_a, y_n, t^k), \qquad U^{x,k}_{i,N_x+1/2,n} = g_i(x_b, y_n, t^k), \tag{3.13}$$

$$U^{y,k}_{1,m,1/2} = -g_1(x_m, y_a, t^k), \qquad U^{y,k}_{2,m,N_y+1/2} = g_2(x_m, y_b, t^k), \tag{3.14}$$

$$U^k_{\gamma,1/2,\widetilde{N}_y+1/2} = g_\gamma(x_a, t^k), \qquad U^k_{\gamma,N_x+1/2,\widetilde{N}_y+1/2} = g_\gamma(x_b, t^k), \tag{3.15}$$

$$P^0_{i,m,n} = p^0_i(x_m, y_n, 0), \tag{3.16}$$

$$P^0_{\gamma,m,\widetilde{N}_y+1/2} = p^0_\gamma(x_m, y_c, 0), \tag{3.17}$$

where

$$\begin{aligned}
&1 \le n \le \widetilde{N}_y \text{ for } i = 1,\ \widetilde{N}_y + 1 \le n \le N_y \text{ for } i = 2,\\
&\quad\text{and } 1 \le m \le N_x \text{ for both } i = 1, 2 \text{ in (3.6)};\\
&1 \le n \le \widetilde{N}_y \text{ for } i = 1,\ \widetilde{N}_y + 1 \le n \le N_y - 1 \text{ for } i = 2,\\
&\quad\text{and } 1 \le m \le N_x - 1 \text{ for both } i = 1, 2 \text{ in (3.7)};\\
&1 \le n \le \widetilde{N}_y - 1 \text{ for } i = 1,\ \widetilde{N}_y + 1 \le n \le N_y - 1 \text{ for } i = 2,\\
&\quad\text{and } 1 \le m \le N_x - 1 \text{ for both } i = 1, 2 \text{ in (3.8)};\\
&1 \le m \le N_x \text{ in (3.9), (3.11), (3.12), (3.17}s\text{)};\\
&1 \le n \le \widetilde{N}_y \text{ for } i = 1,\ \widetilde{N}_y + 1 \le n \le N_y \text{ for } i = 2 \text{ in (3.13)};\\
&1 \le m \le N_x \text{ in (3.14)}; \qquad 1 \le m \le N_x - 1 \text{ in (3.10)};\\
&1 \le n \le \widetilde{N}_y \text{ for } i = 1,\ \widetilde{N}_y + 1 \le n \le N_y \text{ for } i = 2,\\
&\quad\text{and } 1 \le m \le N_x \text{ for both } i = 1, 2 \text{ in (3.16)};\\
&k \ge 1 \text{ for all } k \text{ in (3.6)} - \text{(3.15)}.
\end{aligned}$$

In the above scheme, we place the different degrees of freedom of numerical velocity on the both sides of fracture-interface. As a result, the jump of velocity along the direction normal to fracture, which arises from the velocity across the fracture ($\mathbf{u}_1 \cdot \mathbf{n}_1|_{\Omega_\gamma} + \mathbf{u}_2 \cdot \mathbf{n}_2|_{\Omega_\gamma}$), can be captured easily. This is one of the major advantages of the proposed numerical approach. In order to show the grids with degrees of freedom in Fig. 2, a small thickness of fracture is plotted for the convenience of describing the position of $U^{y,k}_{1,m,\widetilde{N}_y+1/2}$ and $U^{y,k}_{2,m,\widetilde{N}_y+1/2}$, whose values are not equal in general. In both the theoretical analysis and numerical computation, the fracture is considered as one-dimensional interface between two two-dimensional subdomains.

Remark In order to better observe the flow of fluid in fracture-interface, one might need to use smaller grids in the fracture-interface compared with those in the surrounding porous media. This will lead to nonmatching spatial and temporal grids for one-dimensional fracture-interface and two-dimensional surrounding medium. By means of appropriate interpolation and extrapolation operators in space and time, we can adapt the proposed finite difference scheme to the nonmatching grids in Section 3.2.

3.2 Extension to nonmatching grids

In this subsection, we extend the block-centered finite difference method to nonmatching grids in both space and time.

Considering the fracture acts as a fast path in the aquifer system, the flow moves very rapidly in the fracture. Then, smaller scale of meshes in space and time might be employed in fracture domain than in the surrounding medium in order to simulate the rapid changes of flow velocity and pressure in the fracture. Such requirement brings a multi-scale challenge to numerically solve the reduced model, which will

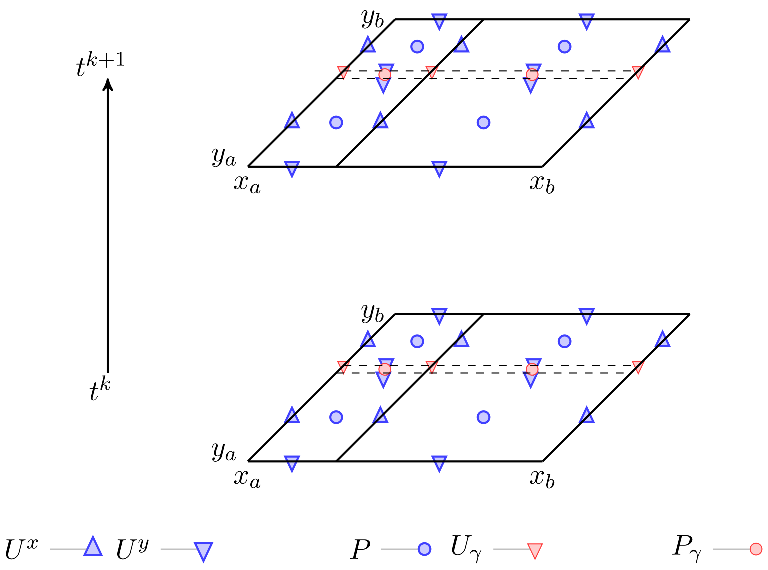

Fig. 2 Grids with labeled degrees of freedom of block-centered scheme

lead to nonmatching spatial and temporal mesh grids. In this subsection, we modify and extend the block-centered finite difference scheme to nonmatching grids in both space and time.

Suppose

$$\Omega_{\gamma h} : x_a = x_{1/2} < x_{3/2} < \cdots < x_{l+1/2} < \cdots < x_{N^x_\gamma - 1/2} < x_{N^x_\gamma + 1/2} = x_b,$$

where $N^x_\gamma > N^x$. Then, the spacial grids of fracture domain do not match those of surrounding porous media (see Fig. 3).

For the purpose of constructing the block-centered finite difference scheme, we define Π^u_i and Π^p_i as the bilinear interpolation and extrapolation operators for Ω_i with $i = 1, 2$. Take Π^u_1 and Π^p_1 for example:

- For each point $(x, y) \in [x_{1/2}, x_1) \times \{y_{\widetilde{N}_y+1/2}\}$, we define $\Pi^u_1 u^y_1(x, y)$ to be the bilinear extrapolation by using $u^y_{1,1,\widetilde{N}_y+1/2}$, $u^y_{1,2,\widetilde{N}_y+1/2}$, and define $\Pi^p_1 p_1(x, y)$ as the bilinear extrapolation by using $p_{1,1,\widetilde{N}_y+1}$, $p_{1,1,\widetilde{N}_y+2}$, $p_{1,2,\widetilde{N}_y+1}$, $p_{1,2,\widetilde{N}_y+2}$.
- For each point $(x, y) \in [x_m, x_{m+1}] \times \{y_{\widetilde{N}_y+1/2}\}$ with $m = 1, \cdots, N_x - 1$, we define $\Pi^u_1 u^y_1(x, y)$ to be the bilinear interpolation by using $u^y_{1,m,\widetilde{N}_y+1/2}$, $u^y_{1,m+1,\widetilde{N}_y+1/2}$, and define $\Pi^p_1 p_1(x, y)$ as the bilinear extrapolation by using $p_{1,m,\widetilde{N}_y+1}$, $p_{1,m,\widetilde{N}_y+2}$, $p_{1,m+1,\widetilde{N}_y+1}$, $p_{1,m+1,\widetilde{N}_y+2}$.
- For each point $(x, y) \in (x_{N_x}, x_{N_x+1/2}] \times \{y_{\widetilde{N}_y+1/2}\}$, we define $\Pi^u_1 u^y_1(x, y)$ to be the bilinear extrapolation by using $u^y_{1,N_x,\widetilde{N}_y+1/2}$, $u^y_{1,N_x-1,\widetilde{N}_y+1/2}$, and define $\Pi^p_1 p_1(x, y)$ as the bilinear extrapolation by using $p_{1,N_x,\widetilde{N}_y+1}$, $p_{1,N_x,\widetilde{N}_y+2}$, $p_{1,N_x-1,\widetilde{N}_y+1}$, $p_{1,N_x-1,\widetilde{N}_y+2}$.

Similarly, we can define the bilinear operators Π^u_2 and Π^p_2 on $u^y_2(x, y)$ and $p_2(x, y)$, respectively.

When the temporal grids of fracture domain do not match those of surrounding porous media (see Fig. 4), we use t_j with $j = 0, 1, \cdots, N^t_\gamma$ to denote the temporal grids of fracture region and $\Delta t_j = t_j - t_{j-1}$ to represent the time step. In order to preserve accuracy, we set $t_0 = t^0$ and $t_1 = t^1$, and subdivide the remaining part of time grid according to $r\Delta t_j = \Delta t^k$ $(r \in Z^+)$. For $t_j \in (t^k, t^{k+1}]$ with $k \geq 1$, we

Fig. 3 Sketch of nonmatching spatial grids

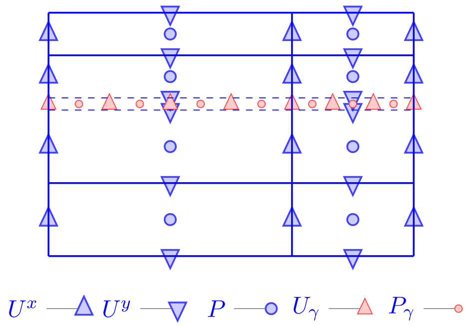

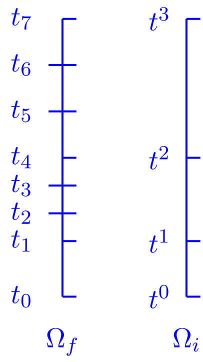

Fig. 4 Sketch of nonmatching temporal grids

define $\Pi^t_\gamma u^{y,j}$ as the linear extrapolation to t_j by using $u^{y,k}$ and $u^{y,k-1}$, and $\Pi^t_\gamma p^j$ as the linear extrapolation to t_j by using p^k and p^{k-1}.

Then, the block-centered finite difference scheme on the nonmatching grids is given to approximate $u^x_i(x_{m+1/2}, y_n, t^k)$, $u^y_i(x_m, y_{n+1/2}, t^k)$, $p_i(x_m, y_n, t^k)$ $(i = 1, 2)$, $u_\gamma(x_{l+1/2}, y_c, t^j)$ and $p_\gamma(x_l, y_c, t^j)$ by $U^{x,k}_{i,m+1/2,n}$, $U^{y,k}_{i,m,n+1/2}$, $P^k_{i,m,n}$ $(i = 1, 2)$, $U^j_{\gamma,l+1/2,\widetilde{N}_y+1/2}$ and $P^j_{\gamma,l,\widetilde{N}_y+1/2}$ as follows:

$$\begin{aligned}
&\phi_\gamma C^F_\gamma [d_t P_\gamma]^j_{l,\widetilde{N}_y+1/2} + [D_x U_\gamma]^j_{l,\widetilde{N}_y+1/2} \\
&\quad = q^j_{\gamma,l,\widetilde{N}_y+1/2} + \Pi^t_\gamma \Pi^u_1 U^{y,j}_{1,l,\widetilde{N}_y+1/2} - \Pi^t_\gamma \Pi^u_2 U^{y,j}_{2,l,\widetilde{N}_y+1/2},
\end{aligned} \tag{3.18}$$

$$\begin{aligned}
&(\mu_\gamma + a^x_\gamma(\overline{P}_\gamma)|U_\gamma|^j_{l+1/2,\widetilde{N}_y+1/2}) U^j_{\gamma,l+1/2,\widetilde{N}_y+1/2} \\
&\quad + K^x_\gamma \delta[d_x P_\gamma]^j_{l+1/2,\widetilde{N}_y+1/2} = 0,
\end{aligned} \tag{3.19}$$

$$\begin{aligned}
&(\mu_\gamma + b_\gamma(P_\gamma)|\widehat{U}_\gamma|^j_{l,\widetilde{N}_y+1/2})(\Pi^t_\gamma \Pi^u_1 U^{y,j}_{1,l,\widetilde{N}_y+1/2} - \Pi^t_\gamma \Pi^u_2 U^{y,j}_{2,l,\widetilde{N}_y+1/2}) \\
&\quad = \frac{\alpha_\gamma}{2\xi - 1}(\Pi^t_\gamma \Pi^p_1 P^j_{1,l,\widetilde{N}_y+1/2} + \Pi^t_\gamma \Pi^p_2 P^j_{2,l,\widetilde{N}_y+1/2} - 2P^j_{\gamma,l,\widetilde{N}_y+1/2}),
\end{aligned} \tag{3.20}$$

$$\begin{aligned}
&(\mu_\gamma + b_\gamma(P_\gamma)|\widehat{U}_\gamma|^j_{\gamma,l,\widetilde{N}_y+1/2})(\Pi^t_\gamma \Pi^u_1 U^{y,j}_{1,l,\widetilde{N}_y+1/2} + \Pi^t_\gamma \Pi^u_2 U^{y,j}_{2,l,\widetilde{N}_y+1/2}) \\
&\quad = \alpha_\gamma(\Pi^t_\gamma \Pi^p_1 P^j_{1,l,\widetilde{N}_y+1/2} - \Pi^t_\gamma \Pi^p_2 P^j_{2,l,\widetilde{N}_y+1/2}),
\end{aligned} \tag{3.21}$$

$$U^j_{\gamma,1/2,\widetilde{N}_y+1/2} = g_\gamma(x_a, t^j), \qquad U^j_{\gamma,N^x_\gamma+1/2,\widetilde{N}_y+1/2} = g_\gamma(x_b, t^j), \tag{3.22}$$

$$P^0_{\gamma,l,\widetilde{N}_y+1/2} = p^0_\gamma(x_l, y_c, 0), \tag{3.23}$$

where the discretized scheme on the surrounding porous media is the same as (3.6)–(3.8), (3.13)–(3.14), (3.16), and

$$\begin{aligned}
&1 \le l \le N^x_\gamma \text{ in (3.18), (3.20), (3.21), (3.23);} \\
&1 \le l \le N^x_\gamma - 1 \text{ in (3.19);} \qquad 1 \le j \le N^t_\gamma \text{ in (3.18)} - \text{(3.22).}
\end{aligned}$$

4 Error estimates

In this section, we derive the prior errors theorem 1 of the block-centered finite difference scheme (3.6)–(3.17) for the reduced coupled model (2.30)–(2.37). Firstly, we give some lemmas.

Lemma 1 *Suppose* $p_i \in L^\infty(0, T; W^{3,\infty}(\Omega_i))$ *for* $i = 1, 2, \gamma$*, then*

$$\frac{\partial p_{i,m+1/2,n}}{\partial x} = [d_x p_i]_{m+1/2,n} - \frac{1}{8}\left[d_x\left((h^x)^2\frac{\partial^2 p_i}{\partial x^2}\right)\right]_{m+1/2,n} + O(h_x^2 + h_y^2)\|p_i\|_{3,\infty}, \tag{4.1}$$

$$\frac{\partial p_{i,m,n+1/2}}{\partial y} = [d_y p_i]_{m,n+1/2} - \frac{1}{8}\left[d_y\left((h^y)^2\frac{\partial^2 p_i}{\partial y^2}\right)\right]_{m,n+1/2} + O(h_x^2 + h_y^2)\|p_i\|_{3,\infty}, \tag{4.2}$$

$$\frac{\partial p_{\gamma,m+1/2,\widetilde{N}_y+1/2}}{\partial x} = [d_x p_\gamma]_{m+1/2,\widetilde{N}_y+1/2} - \frac{1}{8}\left[d_x\left((h^x)^2\frac{\partial^2 p_\gamma}{\partial x^2}\right)\right]_{m+1/2,\widetilde{N}_y+1/2} + O(h_x^2)\|p_\gamma\|_{3,\infty}, \tag{4.3}$$

where

$1 \le n \le \widetilde{N}_y$ *for* $i = 1$, $\widetilde{N}_y + 1 \le n \le N_y - 1$ *for* $i = 2$, *and* $1 \le m \le N_x - 1$ *for both* $i = 1, 2$ *in* (4.1);

$1 \le n \le \widetilde{N}_y - 1$ *for* $i = 1$, $\widetilde{N}_y + 1 \le n \le N_y - 1$ *for* $i = 2$, *and* $1 \le m \le N_x - 1$ *for both* $i = 1, 2$ *in* (4.2);

$$1 \le m \le N_x - 1 \text{ in } (4.3).$$

Proof According to Taylor expansion, we have

$$\begin{aligned}
[d_x p_i]_{m+1/2,n} &= \frac{\partial p_{i,m+1/2,n}}{\partial x} + \frac{1}{h^x_{m+1/2}}\left(\frac{(h^x_{m+1})^2}{8}\frac{\partial^2 p_{i,m+1,n}}{\partial x^2} - \frac{(h^x_m)^2}{8}\frac{\partial^2 p_{i,m,n}}{\partial x^2}\right)\\
&\quad + \frac{1}{2h^x_{m+1/2}}\left(\int_{x_{m+1}}^{x_{m+1/2}}\left(\frac{(h^x_{m+1})^2}{8} - \frac{(x-x_{m+1})^2}{2}\right)\frac{\partial^3 p_i}{\partial x^3}(x, y_n)dx\right.\\
&\qquad\left. - \int_{x_m}^{x_{m+1/2}}\left(\frac{(h^x_m)^2}{8} - \frac{(x-x_m)^2}{2}\right)\frac{\partial^3 p_i}{\partial x^3}(x, y_n)dx\right)\\
&\quad + \frac{1}{h^x_{m+1/2}}\left(\frac{(h^x_{m+1})^2}{8}\left(\frac{\partial^2 p_{i,m+1/2,n}}{\partial x^2} - \frac{\partial^2 p_{i,m+1,n}}{\partial x^2}\right)\right.\\
&\qquad\left. + \frac{(h^x_m)^2}{8}\left(\frac{\partial^2 p_{i,m,n}}{\partial x^2} - \frac{\partial^2 p_{i,m+1/2,n}}{\partial x^2}\right)\right)\\
&= \frac{\partial p_{i,m+1/2,n}}{\partial x} - \frac{1}{8}\left[d_x\left((h^x)^2\frac{\partial^2 p_i}{\partial x^2}\right)\right]_{m+1/2,n} + O(h_x^2 + h_y^2)\|p_i\|_{3,\infty},
\end{aligned}$$

where $1 \le n \le \widetilde{N}_y$ for $i = 1$, $\widetilde{N}_y + 1 \le n \le N_y - 1$ for $i = 2$, and $1 \le m \le N_x - 1$ for both $i = 1, 2$.

And

$$
\begin{aligned}
[d_y p_i]_{m,n+1/2} &= \frac{\partial p_{i,m,n+1/2}}{\partial y} + \frac{1}{h^y_{n+1/2}} \left(\frac{(h^y_{n+1})^2}{8} \frac{\partial^2 p_{i,m,n+1}}{\partial y^2} - \frac{(h^y_n)^2}{8} \frac{\partial^2 p_{i,m,n}}{\partial y^2} \right) \\
&\quad + \frac{1}{2h^y_{n+1/2}} \left(\int_{y_{n+1}}^{y_{n+1/2}} \left(\frac{(h^y_{n+1})^2}{8} - \frac{(y-y_{n+1})^2}{2} \right) \frac{\partial^3 p_i}{\partial y^3}(x_m, y) dx \right. \\
&\qquad \left. - \int_{y_n}^{y_{n+1/2}} \left(\frac{(h^y_n)^2}{8} - \frac{(y-y_n)^2}{2} \right) \frac{\partial^3 p_i}{\partial y^3}(x_m, y) dx \right) \\
&\quad + \frac{1}{h^y_{n+1/2}} \left(\frac{(h^y_{n+1})^2}{8} \left(\frac{\partial^2 p_{i,m,n+1/2}}{\partial y^2} - \frac{\partial^2 p_{i,m,n+1}}{\partial y^2} \right) \right. \\
&\qquad \left. + \frac{(h^y_n)^2}{8} \left(\frac{\partial^2 p_{i,m,n}}{\partial y^2} - \frac{\partial^2 p_{i,m,n+1/2}}{\partial y^2} \right) \right) \\
&= \frac{\partial p_{i,m,n+1/2}}{\partial y} - \frac{1}{8} \left[d_y \left((h^y)^2 \frac{\partial^2 p_i}{\partial y^2} \right) \right]_{m,n+1/2} + O(h_x^2 + h_y^2) \| p_i \|_{3,\infty},
\end{aligned}
$$

where $1 \le l \le \widehat{N_y} - 1$ for $i = 1$, $\widehat{N_y} + 1 \le l \le N_y - 1$ for $i = 2$, and $1 \le s \le N_x - 1$ for both $i = 1, 2$.

Similarly, we can obtain (4.3). □

The following lemma follows directly from Lemma 1.

Lemma 2 *Suppose $p_i \in L^\infty(0, T; W^{3,\infty}(\Omega_i))$ for $i = 1, 2, \gamma$, then*

$$
u^x_{i,m+1/2,n} = -K^x_i [d_x(p_i - \eta_i)]_{m+1/2,n} + O(h_x^2 + h_y^2) \| p_i \|_{3,\infty}, \tag{4.4}
$$

$$
u^y_{i,m,n+1/2} = -K^y_i [d_y(p_i - \eta_i)]_{m,n+1/2} + O(h_x^2 + h_y^2) \| p_i \|_{3,\infty}, \tag{4.5}
$$

$$
\begin{aligned}
&\mu_\gamma u_{\gamma,m+1/2,\widetilde{N}_y+1/2} + (a^x_\gamma(p_\gamma)|u_\gamma|u_\gamma)_{m+1/2,\widetilde{N}_y+1/2} \\
&= -K^x_\gamma \delta [d_x(p_\gamma - \eta_\gamma)]_{m+1/2,\widetilde{N}_y+1/2} + O(h_x^2) \| p_\gamma \|_{3,\infty},
\end{aligned} \tag{4.6}
$$

where

$$
\eta_{i,m,n} = \frac{1}{8} \left((h^x)^2 \frac{\partial^2 p_i}{\partial x^2} + (h^y)^2 \frac{\partial^2 p_i}{\partial y^2} \right)_{m,n}, \tag{4.7}
$$

$$
\eta_{\gamma,m,\widetilde{N}_y+1/2} = \frac{1}{8} \left((h^x)^2 \frac{\partial^2 p_\gamma}{\partial x^2} \right)_{m,\widetilde{N}_y+1/2}, \tag{4.8}
$$

and

$1 \le n \le \widetilde{N}_y$ *for* $i = 1$, $\widetilde{N}_y + 1 \le n \le N_y - 1$ *for* $i = 2$, *and* $1 \le m \le N_x - 1$ *for both* $i = 1, 2$ *in* (4.4);

$1 \le n \le \widetilde{N}_y - 1$ *for* $i = 1$, $\widetilde{N}_y + 1 \le n \le N_y - 1$ *for* $i = 2$, *and* $1 \le m \le N_x - 1$ *for both* $i = 1, 2$ *in* (4.5);

$$
1 \le m \le N_x - 1 \textit{ in } (4.6).
$$

Lemma 3 *If $p_i \in L^\infty(0,T;W^{3,\infty}(\Omega_i))$ and $u_i \in L^\infty(0,T;W^{3,\infty}(\Omega_i))$ for $i = 1,2,\gamma$, then it holds that*

$$\begin{aligned} & s_i[d_t\tilde{p}_i]^k_{m,n} + [D_x u_i^x]^k_{m,n} + [D_y u_i^y]^k_{m,n} \\ &= q^k_{i,m,n} + O(\Delta t)\|p_i^k\|_{2,\infty} + O(h_x^2+h_y^2)(\|u_i^{x,k}\|_{3,\infty} + \|u_i^{y,k}\|_{3,\infty} + \|p_i^k\|_{3,\infty}), \end{aligned} \tag{4.9}$$

$$\begin{aligned} & \phi_\gamma C_\gamma^F[d_t\tilde{p}_\gamma]^k_{m,\widetilde{N}_y+1/2} + [D_x u_\gamma]^k_{m,\widetilde{N}_y+1/2} - (u^{y,k}_{1,m,\widetilde{N}_y+1/2} - u^{y,k}_{2,m,\widetilde{N}_y+1/2}) \\ &= q^k_{\gamma,m,\widetilde{N}_y+1/2} + O(\Delta t)\|p_\gamma^k\|_{2,\infty} + O(h_x^2)(\|u_\gamma^k\|_{3,\infty} + \|p_\gamma^k\|_{3,\infty}), \end{aligned} \tag{4.10}$$

where $\tilde{p}_i = p_i - \eta_i$ with $i = 1,2$ and $\tilde{p}_\gamma = p_\gamma - \eta_\gamma$, and

$1 \le n \le \widetilde{N}_y$ *for* $i = 1$, $\widetilde{N}_y + 1 \le n \le N_y$ *for* $i = 2$, *and* $1 \le m \le N_x$ *for both* $i = 1,2$ *in* (4.9);
$1 \le m \le N_x$ *in* (4.10).

Proof By the definitions of operators d_t, D_x and D_y, we have

$$\begin{aligned} & s_i[d_t\tilde{p}_i]^k_{m,n} + [D_x u_i^x]^k_{m,n} + [D_y u_i^y]^k_{m,n} \\ &= q^k_{i,m,n} + s_i[d_t(p_i-\eta_i)]^k_{m,n} - s_i\frac{\partial p^k_{i,m,n}}{\partial t} \\ &\quad + [D_x u_i^x]^k_{m,n} - \frac{\partial u^{x,k}_{i,m,n}}{\partial x} + [D_y u_i^y]^k_{m,n} - \frac{\partial u^{y,k}_{i,m,n}}{\partial y} \\ &= q^k_{i,m,n} + O(\Delta t)\|p_i^k\|_{2,\infty} + O(h_x^2+h_y^2)\|p_i^k\|_{3,\infty} \\ &\quad + O(h_x^2)\|u_i^{x,k}\|_{3,\infty} + O(h_y^2)\|u_i^{y,k}\|_{3,\infty}, \end{aligned} \tag{4.11}$$

and

$$\begin{aligned} & \phi_\gamma C_\gamma^F[d_t\tilde{p}_\gamma]^k_{m,\widetilde{N}_y+1/2} + [D_x u_\gamma]^k_{m,\widetilde{N}_y+1/2} - (u^{y,k}_{1,m,\widetilde{N}_y+1/2} - u^{y,k}_{2,m,\widetilde{N}_y+1/2}) \\ &= q^k_{\gamma,m,\widetilde{N}_y+1/2} + \phi_\gamma C_\gamma^F[d_t(p_\gamma-\eta_\gamma)]^k_{m,\widetilde{N}_y+1/2} - \phi_\gamma C_\gamma^F\frac{\partial p^k_{\gamma,m,\widetilde{N}_y+1/2}}{\partial t} \\ &\quad + [D_x u_\gamma]^k_{m,\widetilde{N}_y+1/2} - \frac{\partial u^k_{\gamma,m,\widetilde{N}_y+1/2}}{\partial x} \\ &= q^k_{\gamma,m,\widetilde{N}_y+1/2} + O(\Delta t)\|p_\gamma^k\|_{2,\infty} + O(h_x^2)\|p_\gamma^k\|_{3,\infty} + O(h_x^2)\|u_\gamma^k\|_{3,\infty}. \end{aligned} \tag{4.12}$$

Then, (4.9) and (4.10) follow from (4.11) and (4.12), respectively. □

We refer to Lemma 3.3 in [26] for the proof of the following lemma.

Lemma 4 *Let $W^x_{m+1/2,n}$, $W^y_{m,n+1/2}$, $V^x_{m+1/2,n}$, $V^y_{m,n+1/2}$, $\varphi^x_{m,n}$, and $\varphi^y_{m,n}$ be discrete functions with $V^x_{1/2,n} = V^y_{m,1/2} = V^x_{N_x+1/2,n} = V^y_{m,N_y+1/2} = 0$ and satisfy*

$$\begin{cases} (\psi^x W^x)_{m+1/2,n} = -[d_x\varphi^x]_{m+1/2,n}, \\ (\psi^y W^y)_{m,n+1/2} = -[d_y\varphi^y]_{m,n+1/2}, \end{cases}$$

where ψ^x and ψ^y are generic discrete functions. Then, we have

$$(\psi^x W^x, V^x)_X = (\varphi^x, D_x V^x)_M, \qquad (\psi^y W^y, V^y)_Y = (\varphi^y, D_y V^y)_M.$$

Based on the above lemmas, we give the convergence analysis of the scheme (3.6)–(3.17) for reduced coupled model in the following theorem.

Theorem 1 *Let P_i^k, $U_i^{x,k}$, $U_i^{y,k}$ with $i = 1, 2$ and P_γ^k, U_γ^k be obtained by the block-centered finite difference scheme (3.6)–(3.17). Suppose the coefficients in reduced coupled model are bounded from above and below and the thickness of fracture is small enough, then there exists a positive constant C independent of h_x, h_y, and Δt such that*

$$\begin{aligned}
&\sum_{i=1}^{2} \|P_i^{N_t} - p_i^{N_t}\|_M + \sum_{k=1}^{N_t} \Delta t^k \left(\sum_{i=1}^{2} \|U_i^{x,k} - u_i^{x,k}\|_X^2 + \|U_i^{y,k} - u_i^{y,k}\|_Y^2 \right)^{1/2} \\
\leq\ & C(\Delta t + h_x^2 + h_y^2),
\end{aligned} \tag{4.13}$$

$$\begin{aligned}
&\|P_\gamma^{N_t} - p_\gamma^{N_t}\|_{\gamma M} + \sum_{k=1}^{N_t} \Delta t^k \|U_\gamma^k - u_\gamma^k\|_{\gamma X} \\
\leq\ & C(\Delta t + h_x^2).
\end{aligned} \tag{4.14}$$

Proof Denote

$E_{i,m+1/2,n}^{x,k} = U_{i,m+1/2,n}^{x,k} - u_i^x(x_{m+1/2}, y_n, t^k)$,
with $1 \leq n \leq \widetilde{N}_y$ for $i = 1$, $\widetilde{N}_y + 1 \leq n \leq N_y - 1$ for $i = 2$, and $1 \leq m \leq N_x - 1$ for both i,
$E_{i,m,n+1/2}^{y,k} = U_{i,m,n+1/2}^{y,k} - u_i^y(x_m, y_{n+1/2}, t^k)$,
with $1 \leq n \leq \widetilde{N}_y$ for $i = 1$, $\widetilde{N}_y \leq n \leq N_y - 1$ for $i = 2$, and $1 \leq m \leq N_x - 1$ for both $i = 1, 2$,
$E_{i,m,n}^{p,k} = P_{i,m,n}^k - p_i(x_m, y_n, t^k)$,
with $1 \leq n \leq \widetilde{N}_y$ for $i = 1$, $\widetilde{N}_y + 1 \leq n \leq N_y$ for $i = 2$, and $1 \leq m \leq N_x$ for both $i = 1, 2$,
$e_{\gamma,m+1/2,\widetilde{N}_y+1/2}^{u,k} = U_{\gamma,m+1/2,\widetilde{N}_y+1/2}^k - u_\gamma(x_{m+1/2}, y_{\widetilde{N}_y+1/2}, t^k)$, with $1 \leq m \leq N_x - 1$,
$e_{\gamma,m,\widetilde{N}_y+1/2}^{p,k} = P_{\gamma,m,\widetilde{N}_y+1/2}^k - p_\gamma(x_m, y_{\widetilde{N}_y+1/2}, t^k)$, with $1 \leq m \leq N_x$.

According to Lemma 2, we have

$$E_{i,m+1/2,n}^{x,k} + K_i^x [d_x(E_i^p + \eta_i)]_{m+1/2,n}^k = O(h_x^2 + h_y^2), \tag{4.15}$$

$$E_{i,m,n+1/2}^{y,k} + K_i^y [d_y(E_i^p + \eta_i)]_{m,n+1/2}^k = O(h_x^2 + h_y^2), \tag{4.16}$$

$$\begin{aligned}
&\mu_\gamma e_{\gamma,m+1/2,\widetilde{N}_y+1/2}^{u,k} + (a_\gamma^x(\overline{P}_\gamma)|U_\gamma|U_\gamma)_{m+1/2,\widetilde{N}_y+1/2}^k \\
&-(a_\gamma^x(\overline{p}_\gamma)|u_\gamma|u_\gamma)_{m+1/2,\widetilde{N}_y+1/2}^k + K_\gamma^x \delta [d_x(e_\gamma^p + \eta_\gamma)]_{m+1/2,\widetilde{N}_y+1/2}^k = O(h_x^2),
\end{aligned} \tag{4.17}$$

where $n \neq \widetilde{N}_y$ in (4.16).

Setting $\beta_i^x = 1/K_i^x$, $\beta_i^y = 1/K_i^y$, and $\beta_\gamma = 1/K_\gamma^x \delta$, multiplying (4.15), (4.16), and (4.17) by $E_{i,m+1/2,n}^{x,k} h_{m+1/2}^x h_n^y$, $E_{i,m,n+1/2}^{y,k} h_m^x h_{n+1/2}^y$, and

$e^{u,k}_{\gamma,m+1/2,\widetilde{N}_y+1/2}h^x_{m+1/2}$, respectively, and summing up m and n, we get from Lemma 4 that

$$\sum_{i=1}^{2}\frac{1}{K_i^x}(E_i^{x,k},E_i^{x,k})_X$$
$$=\sum_{i=1}^{2}(E_i^{p,k}+\eta_i^k,D_xE_i^{x,k})_M+\sum_{i=1}^{2}(O(h_x^2+h_y^2),E_i^{x,k})_X, \tag{4.18}$$

$$\sum_{i=1}^{2}\frac{1}{K_i^y}(E_i^{y,k},E_i^{y,k})_Y$$
$$=\sum_{i=1}^{2}(E_i^{p,k}+\eta_i^k,D_yE_i^{y,k})_M+\sum_{i=1}^{2}(O(h_x^2+h_y^2),E_i^{y,k})_Y, \tag{4.19}$$

$$\frac{\mu_\gamma}{K_\gamma^x\delta}(e_\gamma^{u,k},e_\gamma^{u,k})_{\gamma X}+(\frac{\beta_\gamma\rho_\gamma(\overline{P}_\gamma^k)}{\delta}|U_\gamma^k|U_\gamma^k-\frac{\beta_\gamma\rho_\gamma(\overline{p}_\gamma^k)}{\delta}|u_\gamma^k|u_\gamma^k,e_\gamma^{u,k})$$
$$=(e_\gamma^{p,k}+\eta_\gamma^k,D_xe_\gamma^{u,k})_{\gamma M}+(O(h_x^2),e_\gamma^{u,k})_{\gamma X}. \tag{4.20}$$

By applying Lemma 3 and Taylor expansion to (3.6) and (3.9), we have

$$s_i[d_t(E_i^p+\eta_i)]^k_{m,n}+[D_xE_i^x]^k_{m,n}+[D_yE_i^y]^k_{m,n}$$
$$=O(\Delta t+h_x^2+h_y^2), \tag{4.21}$$

$$\phi_fC_\gamma^F[d_t(e_\gamma^p+\eta_\gamma)]^k_{m,\widetilde{N}_y+1/2}+[D_xe_\gamma^u]^k_{m,\widetilde{N}_y+1/2}$$
$$=E^{y,k}_{1,m,\widetilde{N}_y+1/2}-E^{y,k}_{2,m,\widetilde{N}_y+1/2}+O(\Delta t+h_x^2). \tag{4.22}$$

Multiplying (4.21) and (4.22) by $(E_i^p+\eta_i)^k_{m,n}h_m^xh_n^y$ and $(E_\gamma^p+\eta_\gamma)^k_{m,\widetilde{N}_y+1/2}h_m^x$, respectively, and summing up m and n, we have

$$\sum_{i=1}^{2}s_i\left(d_t(E_i^{p,k}+\eta_i^k),E_i^{p,k}+\eta_i^k\right)_M+\phi_\gamma C_\gamma^F\left(d_t(e_\gamma^{p,k}+\eta_\gamma^k),e_\gamma^{p,k}+\eta_\gamma^k\right)_{\gamma M}$$
$$+\sum_{i=1}^{2}(D_xE_i^{x,k},E_i^{p,k}+\eta_i^k)_M+\sum_{i=1}^{2}(D_yE_i^{y,k},E_i^{p,k}+\eta_i^k)_M$$
$$+(D_xe_\gamma^{u,k},e_\gamma^{p,k}+\eta_\gamma^k)_{\gamma M}$$
$$\le(O(\Delta t),E_i^{p,k}+\eta_i^k)_M+(O(h_x^2+h_y^2),E_i^{p,k}+\eta_i^k)_M$$
$$+(E_1^y,e_\gamma^{p,k}+\eta_\gamma^k)_{\gamma M}-(E_2^y,e_\gamma^{p,k}+\eta_\gamma^k)_{\gamma M}+(O(\Delta t+h_x^2),e_\gamma^{p,k}+\eta_\gamma^k)_{\gamma M}. \tag{4.23}$$

It follows from (4.18)–(4.20) and (4.23) that

$$
\begin{aligned}
&\sum_{i=1}^{2} s_i \left(d_t(E_i^{p,k}+\eta_i^k),\, E_i^{p,k}+\eta_i^k\right)_M + \phi_\gamma C_\gamma^F \left(d_t(e_\gamma^{p,k}+\eta_\gamma^k),\, e_\gamma^{p,k}+\eta_\gamma^k\right)_{\gamma M} \\
&+\sum_{i=1}^{2}\left(\frac{1}{K_i^x}(E_i^{x,k}, E_i^{x,k})_X + \frac{1}{K_i^y}(E_i^{y,k}, E_i^{y,k})_Y\right) + \frac{\mu_\gamma}{K_\gamma^x \delta}(e_\gamma^{u,k}, e_\gamma^{u,k})_{\gamma X} \\
&+\left((\frac{\beta_\gamma \rho_\gamma(\overline{P}_\gamma)}{\delta}|U_\gamma|U_\gamma)^k_{m+1/2,\widetilde{N}_y+1/2} - (\frac{\beta_\gamma \rho_\gamma(\overline{P}_\gamma)}{\delta}|u_\gamma|u_\gamma)^k_{m+1/2,\widetilde{N}_y+1/2},\, e_\gamma^{u,k}\right)_{\gamma X} \\
\le\ &\sum_{i=1}^{2}(O(\Delta t), E_i^{p,k}+\eta_i^k)_M + \sum_{i=1}^{2}(O(h_x^2+h_y^2), E_i^{p,k}+\eta_i^k)_M \\
&+(E_1^y, e_\gamma^{p,k}+\eta_\gamma^k)_{\gamma M} - (E_2^y, e_\gamma^{p,k}+\eta_\gamma^k)_{\gamma M} + (O(\Delta t + h_x^2), e_\gamma^{p,k}+\eta_\gamma^k)_{\gamma M} \\
&+\sum_{i=1}^{2}(O(h_x^2+h_y^2), E_i^{x,k})_X + \sum_{i=1}^{2}(O(h_x^2+h_y^2), E_i^{y,k})_Y + (O(h_x^2), e_\gamma^{u,k})_{\gamma X}.
\end{aligned}
\tag{4.24}
$$

Combining (4.24), Cauchy-Schwarz inequality, we arrive at

$$
\begin{aligned}
&\sum_{i=1}^{2}\frac{s_i}{2} d_t \|(E_i^p+\eta_i)^k\|_M^2 + \sum_{i=1}^{2}\frac{s_i \Delta t^k}{2}\|d_t(E_i^p+\eta_i)^k\|_M^2 \\
&+\frac{\phi_\gamma C_\gamma^F}{2} d_t\|(e_\gamma^p+\eta_\gamma)^k\|_{\gamma M}^2 + \frac{\phi_\gamma C_\gamma^F \Delta t^k}{2}\|d_t(e_\gamma^p+\eta_\gamma)^k\|_{\gamma M}^2 \\
&+\sum_{i=1}^{2}\frac{\mu_i}{K_i^x}\|E_i^{x,k}\|_X^2 + \sum_{i=1}^{2}\frac{\mu_i}{K_i^y}\|E_i^{y,k}\|_Y^2 + \frac{\mu_\gamma}{K_\gamma^x\delta}\|e_\gamma^{u,k}\|_{\gamma X}^2 \\
\le\ & C\left((\Delta t + h_x^2 + h_y^2)^2 + \sum_{i=1}^{2}\|E_i^{p,k}+\eta_i^k\|_M^2 + \|e_\gamma^{p,k}+\eta_\gamma^k\|_{\gamma M}^2\right) \\
&+\sum_{i=1}^{2}\frac{\mu_i}{2K_i^x}\|E_i^{x,k}\|_X^2 + \sum_{i=1}^{2}\frac{\mu_i}{2K_i^y}\|E_i^{y,k}\|_Y^2 + \frac{\mu_\gamma}{2K_\gamma^x\delta}\|e_\gamma^{u,k}\|_{\gamma X}^2.
\end{aligned}
\tag{4.25}
$$

Multiplying (4.25) by $2\Delta t^k$ and summing up k from 1 to N_t, we have

$$
\begin{aligned}
&\sum_{i=1}^{2}\|(E_i^p+\eta_i)^{N_t}\|_M^2 + \|(e_\gamma^p+\eta_\gamma)^{N_t}\|_{\gamma M}^2 \\
&+\sum_{i=1}^{2}\sum_{k=1}^{N_t}(\Delta t^k)^2\|d_t(E_i^p+\eta_i)^k\|_M^2 + \sum_{k=1}^{N_t}(\Delta t^k)^2\|d_t(e_\gamma^p+\eta_\gamma)^k\|_{\gamma M}^2 \\
&+\sum_{i=1}^{2}\sum_{k=1}^{N_t}\Delta t^k(\|E_i^{x,k}\|_X^2 + \|E_i^{y,k}\|_Y^2) + \sum_{k=1}^{N_t}\Delta t^k\|e_\gamma^{u,k}\|_{\gamma X}^2 \\
\le\ & C\left((\Delta t + h_x^2+h_y^2)^2 + \sum_{i=1}^{2}\sum_{k=1}^{N_t}\Delta t^k\|E_i^{p,k}+\eta_i^k\|_M^2 + \sum_{k=1}^{N_t}\Delta t^k\|e_\gamma^{p,k}+\eta_\gamma^k\|_{\gamma M}^2\right).
\end{aligned}
\tag{4.26}
$$

Using Gronwall's lemma, we obtain

$$\sum_{i=1}^{2}\|(E_i^p+\eta_i)^{N_t}\|_M^2+\|(e_\gamma^p+\eta_\gamma)^{N_t}\|_{\gamma M}^2$$
$$+\sum_{i=1}^{2}\sum_{k=1}^{N_t}\Delta t^k(\|E_i^{x,k}\|_X^2+\|E_i^{y,k}\|_Y^2)+\sum_{k=1}^{N_t}\Delta t^k\|e_\gamma^{u,k}\|_{\gamma X}^2$$
$$\leq C(\Delta t+h_x^2+h_y^2)^2. \tag{4.27}$$

It follows from (3.4) that

$$|\widehat{u}_\gamma|_{m,\widetilde{N}_y+1/2}^k=|u_\gamma|_{m,\widetilde{N}_y+1/2}^k+O(h_x^2)\|u_\gamma\|_{2,\infty}. \tag{4.28}$$

Combining (2)–(2), (3.11)–(3.12), and (4.28), we have

$$\begin{aligned}
&\mu_\gamma E_{1,m,\widetilde{N}_y+1/2}^{y,k}+(b_\gamma(p_\gamma)|u_\gamma|)_{m,\widetilde{N}_y+1/2}^k E_{1,m,\widetilde{N}_y+1/2}^{y,k}\\
&=(b_\gamma(p_\gamma)|\widehat{U}_\gamma|)_{m,\widetilde{N}_y+1/2}^k U_{1,m,\widetilde{N}_y+1/2}^{y,k}-(b_\gamma(P_\gamma)|\widehat{U}_\gamma|)_{m,\widetilde{N}_y+1/2}^k U_{1,m,\widetilde{N}_y+1/2}^{y,k}\\
&\quad+(b_\gamma(p_\gamma)|\widehat{u}_\gamma|)_{m,\widetilde{N}_y+1/2}^k U_{1,m,\widetilde{N}_y+1/2}^{y,k}-(b_\gamma(p_\gamma)|\widehat{U}_\gamma|)_{m,\widetilde{N}_y+1/2}^k U_{1,m,\widetilde{N}_y+1/2}^{y,k}\\
&\quad+(b_\gamma(p_\gamma)|u_\gamma|)_{m,\widetilde{N}_y+1/2}^k U_{1,m,\widetilde{N}_y+1/2}^{y,k}-(b_\gamma(p_\gamma)|\widehat{u}_\gamma|)_{m,\widetilde{N}_y+1/2}^k U_{1,m,\widetilde{N}_y+1/2}^{y,k}\\
&\quad+\frac{1}{2}(\frac{\alpha_\gamma}{2\xi-1}-\alpha_\gamma)I_2(E_2^p+\eta_2)_{m,\widetilde{N}_y+1/2}^k+\frac{1}{2}(\frac{\alpha_\gamma}{2\xi-1}+\alpha_\gamma)I_1(E_1^p+\eta_1)_{m,\widetilde{N}_y+1/2}^k\\
&\quad-\frac{2\alpha_\gamma}{2\xi-1}(e_\gamma^p+\eta_\gamma)_{m+1/2,\widetilde{N}_y+1/2}^k+O(h_x^2+h_y^2)\|p_i^k\|_{2,\infty},
\end{aligned} \tag{4.29}$$

$$\begin{aligned}
&\mu_\gamma E_{2,m,\widetilde{N}_y+1/2}^{y,k}+(b_\gamma(p_\gamma)|u_\gamma|)_{m,\widetilde{N}_y+1/2}^k E_{2,m,\widetilde{N}_y+1/2}^{y,k}\\
&=(b_\gamma(p_\gamma)|\widehat{U}_\gamma|)_{m,\widetilde{N}_y+1/2}^k U_{2,m,\widetilde{N}_y+1/2}^{y,k}-(b_\gamma(P_\gamma)|\widehat{U}_\gamma|)_{m,\widetilde{N}_y+1/2}^k U_{2,m,\widetilde{N}_y+1/2}^{y,k}\\
&\quad+(b_\gamma(p_\gamma)|\widehat{u}_\gamma|)_{m,\widetilde{N}_y+1/2}^k U_{2,m,\widetilde{N}_y+1/2}^{y,k}-(b_\gamma(p_\gamma)|\widehat{U}_\gamma|)_{m,\widetilde{N}_y+1/2}^k U_{2,m,\widetilde{N}_y+1/2}^{y,k}\\
&\quad+(b_\gamma(p_\gamma)|u_\gamma|)_{m,\widetilde{N}_y+1/2}^k U_{2,m,\widetilde{N}_y+1/2}^{y,k}-(b_\gamma(p_\gamma)|\widehat{u}_\gamma|)_{m,\widetilde{N}_y+1/2}^k U_{2,m,\widetilde{N}_y+1/2}^{y,k}\\
&\quad-\frac{1}{2}(\frac{\alpha_\gamma}{2\xi-1}+\alpha_\gamma)I_2(e_2^p+\eta_2)_{m,\widetilde{N}_y+1/2}^k-\frac{1}{2}(\frac{\alpha_\gamma}{2\xi-1}-\alpha_\gamma)I_1(e_1^p+\eta_1)_{m,\widetilde{N}_y+1/2}^k\\
&\quad-\frac{2\alpha_\gamma}{2\xi-1}(e_\gamma^p+\eta_\gamma)_{m+1/2,\widetilde{N}_y+1/2}^k+O(h_x^2+h_y^2)\|p_i^k\|_{2,\infty}.
\end{aligned} \tag{4.30}$$

Applying (4.27) to (4.29)–(4.30), we have

$$\|E_{1,m,\widetilde{N}_y+1/2}^{y,k}\|_X+\|E_{2,m,\widetilde{N}_y+1/2}^{y,k}\|_X\leq C(h_x^2+h_y^2). \tag{4.31}$$

Finally, the theorem establishes on the basis of (4.7)–(4.8) and (4.27)–(4.31) for the finite difference scheme (3.6)–(3.17) approximating the reduced coupled model. □

Remark Due to the fact the bilinear interpolation and extrapolation operators remain the second-order accuracy, the block-centered finite difference scheme (3.18)–(3.22) on the nonmatching grids for the fracture and surrounding media is without loss of any accuracy.

5 Numerical examples

In this section, some examples are given to illustrate the efficiency and accuracy of the coupled finite difference method for the reduced coupled model. In order to observe the influence of parameter ξ on the flow of fluid, we take different values of ξ in the reduced coupled model to compare the results. Several experiments are performed to analyze the roles of the permeability tensor of the fracture in affecting the flow rate of fluid.

All test cases in this section are based on the following reduced coupled model (cf. (2)–(2)),

$$\left\{\begin{array}{ll} \partial_t p_i + \mathrm{div}\mathbf{u}_i = q_i, & \text{in } \Omega_i \times J, \quad i=1,2, \\ \mathbf{u}_i + \nabla p_i = G_i, & \text{in } \Omega_i \times J, \quad i=1,2, \\ \partial_t p_\gamma + \mathrm{div}_x u_\gamma = q_\gamma + (\mathbf{u}_1\cdot\mathbf{n}_1|_{\Omega_\gamma} + \mathbf{u}_2\cdot\mathbf{n}_2|_{\Omega_\gamma}), & \text{on } \Omega_\gamma \times J, \\ (1+\dfrac{K_\gamma^x\beta_\gamma\rho_\gamma(p_\gamma)}{\delta}|u_\gamma|)u_\gamma + K_\gamma^x\delta\nabla_\tau p_\gamma = G_\gamma, & \text{on } \Omega_\gamma \times J, \\ -\xi(\mu_\gamma + \frac{\alpha_\gamma\beta_\gamma\rho_\gamma(p_\gamma)|u_\gamma|}{2})\mathbf{u}_1\cdot\mathbf{n}_1|_{\Omega_\gamma} + \alpha_\gamma p_1|_{\Omega_\gamma} & \\ \qquad = -(1-\xi)(\mu_\gamma + \frac{\alpha_\gamma\beta_\gamma\rho_\gamma(p_\gamma)|u_\gamma|}{2})\mathbf{u}_2\cdot\mathbf{n}_2|_{\Omega_\gamma} + \alpha_\gamma p_\gamma, & \text{on } \Omega_\gamma \times J, \\ -\xi(\mu_\gamma + \frac{\alpha_\gamma\beta_\gamma\rho_\gamma(p_\gamma)|u_\gamma|}{2})\mathbf{u}_2\cdot\mathbf{n}_2|_{\Omega_\gamma} + \alpha_\gamma p_2|_{\Omega_\gamma} & \\ \qquad = -(1-\xi)(\mu_\gamma + \frac{\alpha_\gamma\beta_\gamma\rho_\gamma(p_\gamma)|u_\gamma|}{2})\mathbf{u}_1\cdot\mathbf{n}_1|_{\Omega_\gamma} + \alpha_\gamma p_\gamma, & \text{on } \Omega_\gamma \times J, \\ \mathbf{u}_i\cdot\nu_i = g_i, & \text{on } \Gamma \times J, \quad i=1,2,\gamma, \\ p_i(\cdot,0) = p_i^0, & \text{in } \Omega_i, \quad i=1,2,\gamma, \end{array}\right. \tag{5.1}$$

where $\alpha_\gamma = 2K_\gamma^y/\delta$.

In this section, we shall solve the reduced coupled model (5.1) by block-centered finite difference scheme on the following domain, as shown in Fig. 5. The values of other parameters are given in the examples.

5.1 Test cases for convergence rates

In this subsection, one example is given to demonstrate the convergence rate of finite difference method for the reduced coupled model (5.1). Let h be the maximum of

Fig. 5 The figure of whole domain

Table 1 Errors for reduced coupled model on nonuniform mesh when $t = 0.5$

Mesh	h	$\|E^p\|_M$	$\|E^u\|_{XY}$	$\|e_\gamma^p\|_{\gamma M}$	$\|e_\gamma^u\|_{\gamma X}$
4×4	3.7500e−01	6.3813e−01	2.1479e−01	4.5191e−01	8.6113e−06
8×8	1.8750e−01	1.3654e−01	5.1204e−02	9.3760e−02	2.0991e−06
16×16	9.3750e−02	3.2887e−02	1.2617e−02	2.2161e−02	5.6654e−07
32×32	4.6875e−02	8.1481e−03	3.1433e−03	5.4495e−03	1.5594e−07
64×64	2.3438e−02	2.0325e−03	7.8517e−04	1.3560e−03	4.3420e−08
	rate	2.0656	2.0217	2.0866	1.9014

h_x and h_y, and E^p, E^u, e_γ^p, e_γ^u denote the prior errors obtained by block-centered finite difference method (3.6)–(3.17) to the example model. The temporal mesh size is chosen that $\Delta t = h^2$ in all examples on the nonuniform rectangular grids.

Example 1 We determine the right-hand side functions and initial boundary conditions according to the following analytic solutions

$$\begin{cases} u_\gamma = x(1-x), & \text{on } \Omega_\gamma \times J, \\ p_\gamma = t\sin(2\pi x) - (3t\sin(2\pi x)(50x(x-1)-1))/1000, & \text{on } \Omega_\gamma \times J, \\ p_1 = t\sin(2\pi x)(y+1), & \text{in } \Omega_1 \times J, \\ p_2 = -t\sin(2\pi x)(y-1), & \text{in } \Omega_2 \times J, \end{cases} \tag{5.2}$$

where $J = (0, 0.5]$, $\mathbb{K}_\gamma = 0.1\mathbb{I}$, $\beta_\gamma = 0.5$, $\rho_\gamma = 1$, $\xi = 4/5$.

The errors obtained by using finite difference scheme (3.6)–(3.17) to solve the reduced coupled model are listed in Table 1. We compute the errors by using the definitions of norms.

The a priori errors for pressure and velocity in the discrete relative L^2 norms and their corresponding convergence rates are listed in Tables 1 for reduced coupled example 1. The convergence rates are obtained by applying a least-square fitting method to the numerical errors with respect to the mesh sizes h. From Table 1, it can be seen that the proposed finite difference approximation has second-order accuracy in discrete L^2 norms for both pressure and velocity, which is consistent with the theoretical results in Theorem 1.

5.2 Test cases for influence of ξ

We have assumed that the range of parameter ξ is from 1/2 to 1 in Section 2. In this subsection, we check the influence of value ξ on the flow of fluid in fractured system. In Example 2, we compare numerical results obtained by changing the value of parameter ξ while keeping other parameters unchanged.

Example 2 Consider a practical model in time interval $J = (0, 1]$. Here, we choose the following right-hand side functions and initial boundary conditions:

$$\begin{cases} G_1 = 0, & \text{in } \Omega_1 \times J, \\ G_2 = 0, & \text{in } \Omega_2 \times J, \\ G_\gamma = 0, & \text{on } \Omega_\gamma \times J, \\ q_\gamma = 0, & \text{on } \Omega_\gamma \times J, \\ q_1 = 0, & \text{in } \Omega_1 \times J, \\ q_2 = 0, & \text{in } \Omega_2 \times J, \\ u_\gamma(0) = u_\gamma(1) = 0; & \\ u_1 \cdot \nu_1|_{y=-0.5} = 1; & \\ u_1 \cdot \nu_1|_{x=0} = -1, & \\ u_1 \cdot \nu_1|_{x=1} = 1, & \\ u_2 \cdot \nu_2|_{y=0.5} = -1, & \\ u_2 \cdot \nu_2|_{x=0} = -1, & \\ u_2 \cdot \nu_2|_{x=1} = 1, & \\ p_1(\cdot, 0) = 0, & \text{in } \Omega_1 \times J, \\ p_2(\cdot, 0) = 0, & \text{in } \Omega_2 \times J, \\ p_\gamma(\cdot, 0) = 0, & \text{on } \Omega_\gamma \times J, \end{cases} \tag{5.3}$$

where $\beta_i = 3, \rho_i = 1 (i = 1, 2, \gamma)$ in the fractured media aquifer system (5.1). The fracture is assumed to be anisotropic.

The numerical results on nonuniform staggered meshes obtained by different values of ξ are plotted in Figs. 6 and 7 and Figs. 8 and 9 for reduced coupled model. From the numerical results, it is clear to see that the value of parameter ξ has little influence on the flow rate of fluid for reduced coupled model, which is independent of the permeability tensor of the fracture.

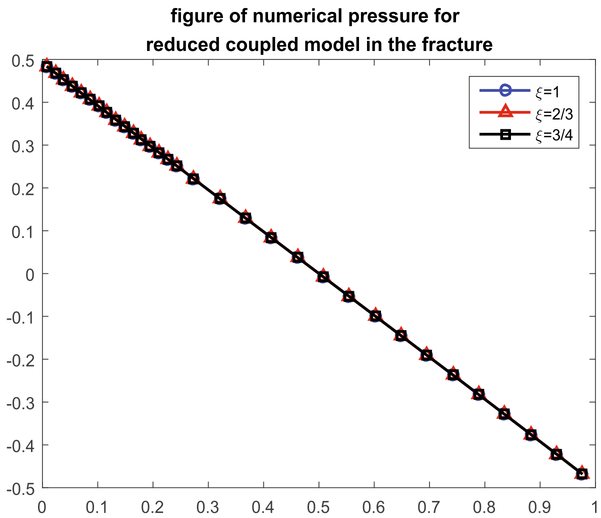

Fig. 6 Plots of numerical pressure solutions for Example 2 with $K_\gamma^x = 0.1$ and $K_\gamma^y = 100$ when $t = 1$

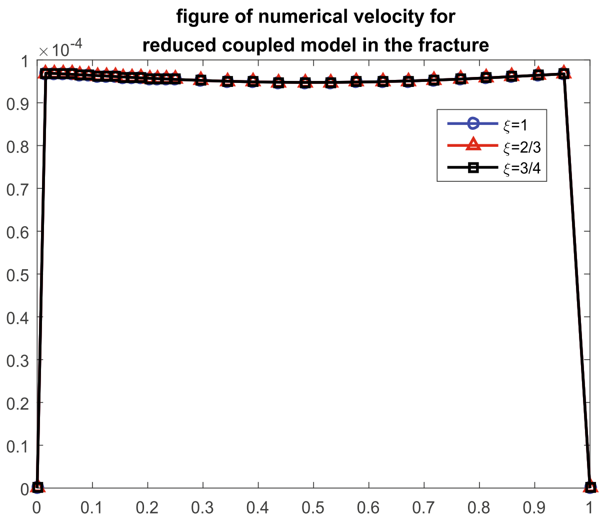

Fig. 7 Plots of numerical velocity solutions for Example 2 with $K_\gamma^x = 0.1$ and $K_\gamma^y = 100$ when $t = 1$

5.3 Test cases for the impact of permeability tensor in fracture

In practice, the source of contaminants often occur on and near the ground surface. We will simulate this behavior in Example 3 by introducing one source term at the top of the the whole domain.

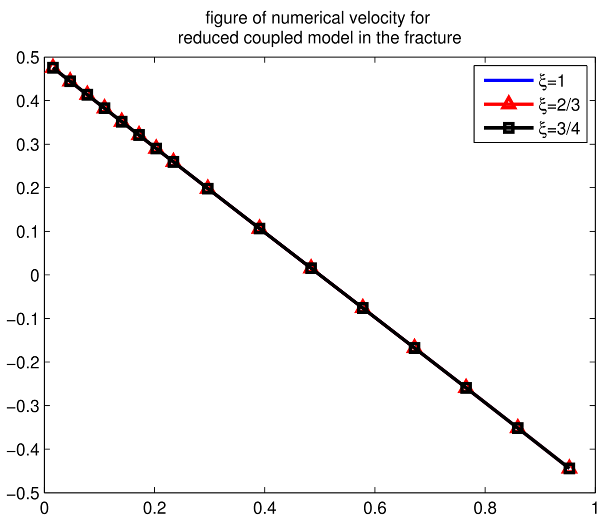

Fig. 8 Plots of numerical pressure solutions for Example 2 with $K_\gamma^x = 100$ and $K_\gamma^y = 0.1$ when $t = 1$

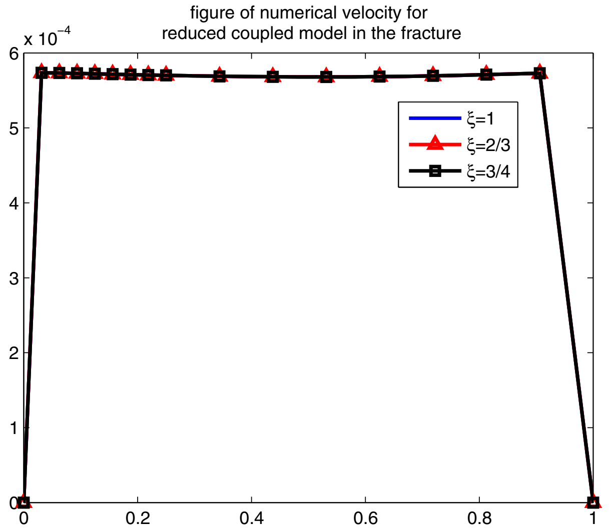

Fig. 9 Plots of numerical velocity solutions for Example 2 with $K_\gamma^x = 100$ and $K_\gamma^y = 0.1$ when $t = 1$

Example 3 Consider a practical model in time interval $J = (0, 1]$. Here, we choose the following right-hand side functions and initial boundary conditions:

$$
\begin{cases}
G_1 = 0, & \text{in } \Omega_1 \times J,\\
G_2 = 0, & \text{in } \Omega_2 \times J,\\
G_\gamma = 0, & \text{on } \Omega_\gamma \times J,\\
q_\gamma = 0, & \text{on } \Omega_\gamma \times J,\\
q_1 = 0, & \text{in } \Omega_1 \times J,\\
q_2 = 10(|(x-0.5)^2 + (y-0.5)^2| < 0.1), & \text{in } \Omega_2 \times J,\\
u_\gamma(0) = u_\gamma(1) = 0; & \\
u_1 \cdot \nu_1|_{y=-0.5} = 0; & \\
u_1 \cdot \nu_1|_{x=0} = -1, & \\
u_1 \cdot \nu_1|_{x=1} = 0, & \\
u_2 \cdot \nu_2|_{y=0.5} = 0, & \\
u_2 \cdot \nu_2|_{x=0} = -1, & \\
u_2 \cdot \nu_2|_{x=1} = 0, & \\
p_1(\cdot, 0) = 0, & \text{in } \Omega_1 \times J,\\
p_2(\cdot, 0) = 0, & \text{in } \Omega_2 \times J,\\
p_\gamma(\cdot, 0) = 0, & \text{on } \Omega_\gamma \times J,
\end{cases}
\tag{5.4}
$$

where $\xi = \frac{4}{5}$, $\rho_\gamma = 1$ in the model (5.1).

We report the numerical results in Figs. 10, 11, 12, 13, and 14. The flux exchanging between the surrounding porous media and fracture-interface is shown to have clear impact on the fluid flow. When the thickness of fracture is fixed, the permeability tensor plays an important role in affecting the fluid flow inside the fracture. More precisely, when the permeability along normal direction of fracture is bigger, the flow rate in surrounding porous media is higher due to exchanging flux with the fracture.

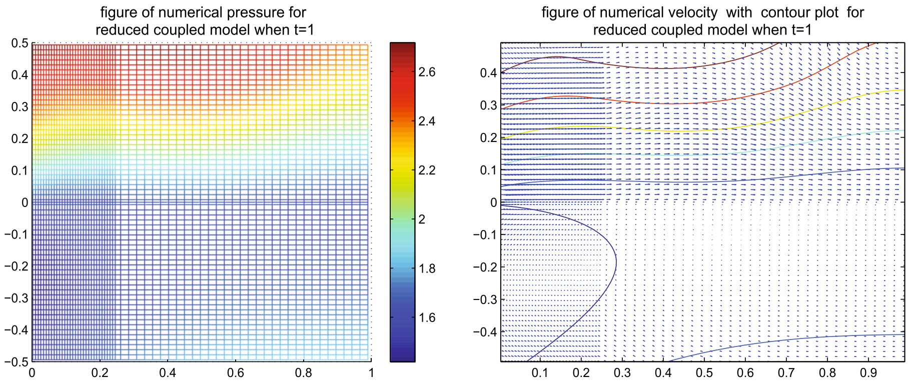

Fig. 10 Plots of numerical solutions for reduced coupled Example 3 with $\mathbb{K}_\gamma = 100\mathbb{I}$ when $t = 1$. Left: the figure of numerical pressure solution in surrounding porous media. Right: the figure of numerical velocity solution in surrounding porous media

If the permeability along tangential direction of fracture is bigger, the flow rate in fracture is higher, which is consistent with the physical phenomenon.

5.4 Comparison of Darcy fracture model with Forchheimer fracture model

In order to demonstrate the influence of the Forchheimer fracture in Karst aquifer system, a comparison of the reduced model presented in this paper with the Darcy model in [12] is given in this subsection. We still use Example 3 to show the differences of numerical solutions of the two models.

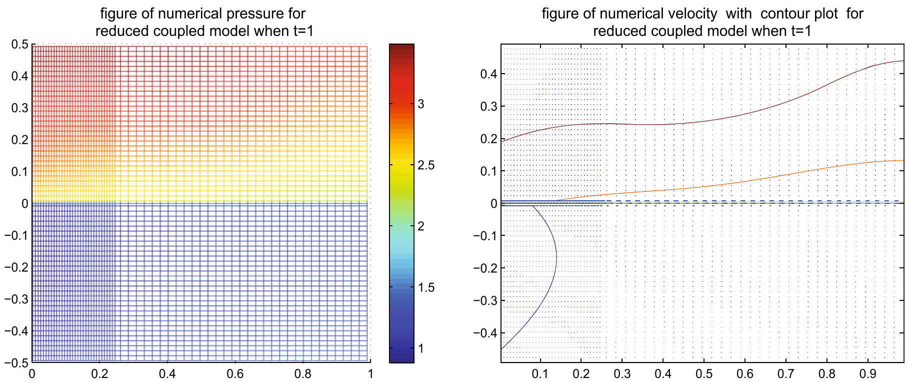

Fig. 11 Plots of numerical solutions for reduced coupled Example 3 with $K_\gamma^x = 100$ and $K_\gamma^y = 0.001$ when $t = 1$. Left: the figure of numerical pressure solution in surrounding porous media. Right: the figure of numerical velocity solution in surrounding porous media

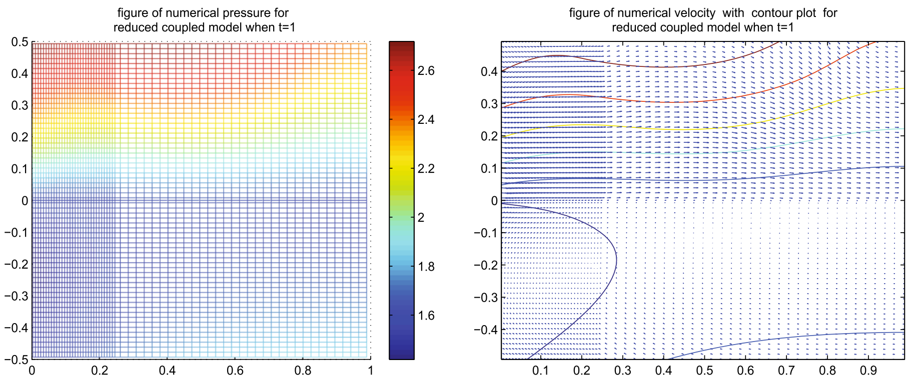

Fig. 12 Plots of numerical solutions for reduced coupled Example 3 with $K_\gamma^x = 0.001$ and $K_\gamma^y = 100$ when $t = 1$. Left: the figure of numerical pressure solution in surrounding porous media. Right: the figure of numerical velocity solution in surrounding porous media

By testing the different values of permeability tensor in the fracture, it can be seen that there are few differences between the two models when the value of K_f^y is big and there are some differences when the the value of K_f^x is big. From Figs. 15 and 16, we observe that the pressure shows different behavior in the fracture. The pressures in the Forchheimer fracture change more than those in the Darcy fracture. Moreover, we can also observe that the velocity in the former case changes more rapidly that in the latter one.

From the above numerical tests, one can also observe that the pressure and velocity show different behavior on two sides of fracture-interface. Therefore, our idea of allocating different degrees of freedom on the two sides of fracture-interface is efficient for solving the reduced coupled model.

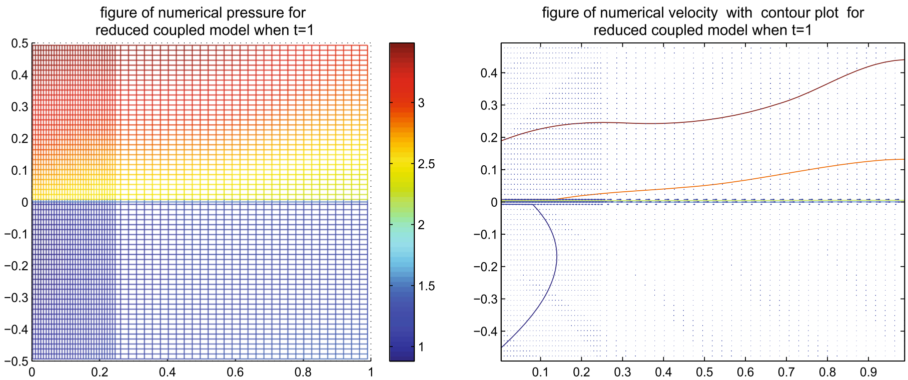

Fig. 13 Plots of numerical solutions for reduced coupled Example 3 with $\mathbb{K}_\gamma = 0.001\mathbb{I}$ when $t = 1$. Left: the figure of numerical pressure solution in surrounding porous media. Right: the figure of numerical velocity solution in surrounding porous media

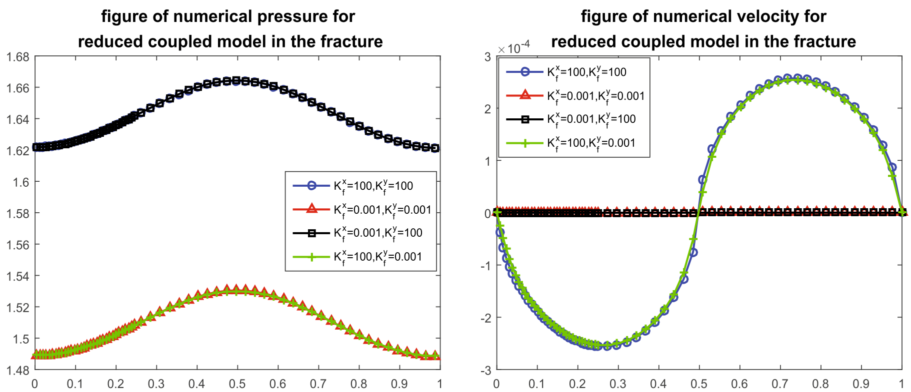

Fig. 14 Plots of numerical solutions for reduced coupled Example 3 with different $\mathbb{K}_\gamma$ when $t = 1$. Left: the figure of numerical pressure solution in the fracture. Right: the figure of numerical velocity solution in the fracture

6 Conclusions

In this paper, we consider reduced coupled model with different dimensions in fractured media aquifer system. The Forchheimer's law is employed for modeling the flow in the fracture. The flow in the surrounding domain follows Darcy's law. The fracture is treated as an interface due to its relatively small thickness, which leads to reduced coupled model. The nonlinear exchanging condition is imposed on the fracture-interface. A block-centered finite difference scheme is designed to approximate the flux transmission condition on the fracture-interface without requiring continuities in pressure and velocity. It is proved theoretically and demonstrated numerically that the block-centered finite difference method preserves second-order accuracy for both pressure and velocity. Moreover, we show the permeability tensor in the fracture has an important impact on the flow rate in both the surrounding porous

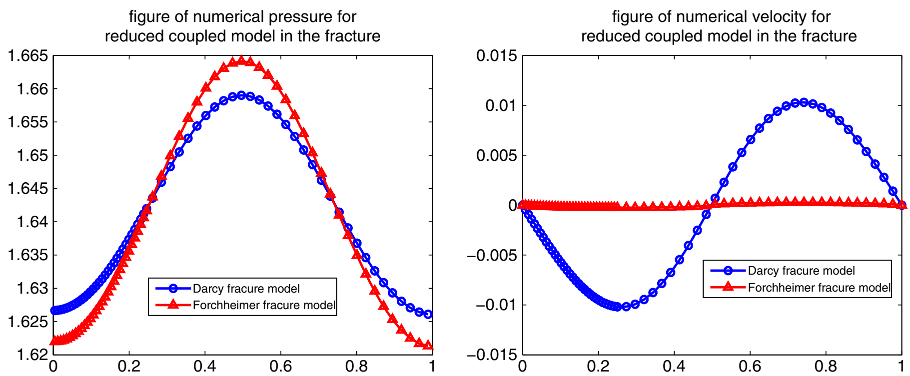

Fig. 15 Plots of numerical solutions for Example 3 with $\mathbb{K}_\gamma = 100\mathbb{I}$ when $t = 1$. Left: the figure of numerical pressure solution in the fracture. Right: the figure of numerical velocity solution in the fracture

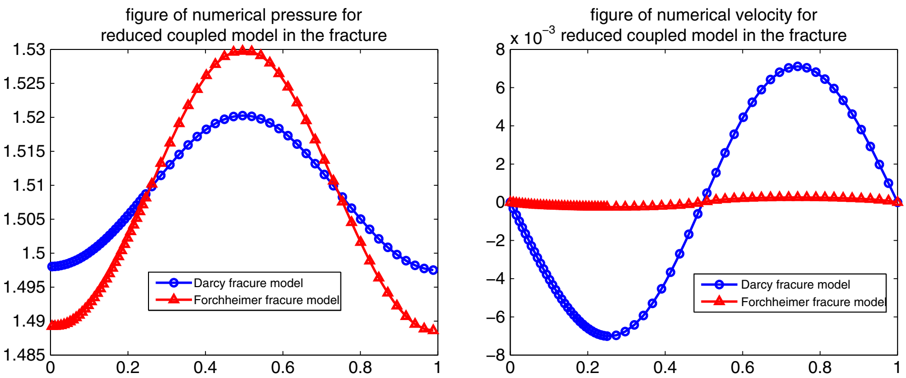

Fig. 16 Plots of numerical solutions for Example 3 with $K_\gamma^x = 100$ and $K_\gamma^y = 0.001$ when $t = 1$. Left: the figure of numerical pressure solution in the fracture. Right: the figure of numerical velocity solution in the fracture

media and fracture-interface. It is observed that the tangential direction of permeability tensor determines that flow rate in the fracture and the normal one determines the flow rate in the surrounding porous media. By using high-order interpolation and extrapolation operators, it is easy to extend the numerical procedure to the nonmatching spatial and temporal grids in the whole domain without losing any accuracy. Our future work is to consider the multiple Forchheimer fractures with orientations by referring to [30, 31].

Funding information The work is supported by the National Natural Science Foundation of China Grant No. 11771367, the Shandong Provincial Natural Science Foundation No. ZR2019MA049, Shandong Province Higher Educational Science and Technology Program No. J16LI05 and The Hong Kong RGC General Research Fund, Grant No. 15302518.

References

1. Bauer, S., Liedl, R., Sauter, M.: Modeling of karst aquifer genesis: influence of exchange flow. Water Resour. Res. **39**(10), 371–375 (2003)
2. Bauer, S., Liedl, R., Sauter, M., Stauffer, F., Kinzelbach, W., Kovar, K., Hoehn, E.: Modelling of karst development considering conduit-matrix exchange flow, in Calibration and reliability in groundwater modelling: coping with uncertainty. In: Proceedings of the ModelCARE'99 conference held in Zurich, Switzerland, 20-23 September, 1999 (2000)
3. Birk, S., Liedl, R., Sauter, M., Teutsch, G.: Hydraulic boundary conditions as a controlling factor in karst genesis: a numerical modeling study on artesian conduit development in gypsum. Water Resour. Res. **39**(1), SBH 2–1–SBH 2–14 (2003)
4. Espinosa-Paredes, G., Morales-Zárate, E., Vázquez-Rodríguez, A.: Analytical analysis for mass transfer in a fractured porous medium. Pet. Sci. Technol. **31**(19), 2004–2012 (2013)
5. Aulisa, E., Ibragimov, A., Valko, P., Walton, J.: Mathematical framework of the well productivity index for fast Forchheimer (non-Darcy) flows in porous media. Math. Models Methods Appl. Sci. **19**(08), 1241–1275 (2009)
6. Aulisa, E., Bloshanskaya, L., Hoang, L., Ibragimov, A.: Analysis of generalized Forchheimer flows of compressible fluids in porous media. J. Math. Phys. **50**(10), 103102 (2009)
7. Forchheimer, P.: Wasserbewegung durch boden. Z. Ver. Deutsch. Ing **45**(1782), 1788 (1901)

8. Ruth, D., Ma, H.: On the derivation of the Forchheimer equation by means of the averaging theorem. Transp. Porous Media **7**(3), 255–264 (1992)
9. Angot, P., Boyer, F., Hubert, F.: Asymptotic and numerical modelling of flows in fractured porous media. ESAIM: Math. Model. Numer. Anal. **43**(2), 239–275 (2009)
10. Fumagalli, A., Scotti, A.: Numerical modelling of multiphase subsurface flow in the presence of fractures. Commun. Appl. Indus. Math. **3**, 1 (2011)
11. Faille, I., Fumagalli, A., Jaffré, J., Roberts, J.E.: Model reduction and discretization using hybrid finite volumes for flow in porous media containing faults. Comput. Geosci. **20**(2), 317–339 (2016)
12. Hoang, T.-T.-P., Japhet, C., Kern, M., Roberts, J.E.: Space-time domain decomposition for reduced fracture models in mixed formulation. SIAM J. Numer. Anal. **54**(1), 288–316 (2016)
13. Martin, V., Jaffré, J., Roberts, J.E.: Modeling fractures and barriers as interfaces for flow in porous media. SIAM J. Sci. Comput. **26**(5), 1667–1691 (2005)
14. Frih, N., Martin, V., Roberts, J.E., Saâda, A.: Modeling fractures as interfaces with nonmatching grids. Comput. Geosci. **16**(4), 1043–1060 (2012)
15. Loper, D.E.: An analytic benchmark test for karst-aquifer flow. Geophys. Astrophys. Fluid Dyn. **107**(5), 587–602 (2013)
16. Yao, B., Wei, J., Wang, D., Ma, D., Chen, Z.: Numerical study on seepage property of karst collapse columns under particle migration. CMES: Comput. Model. Eng. Sci. **91**(2), 81–100 (2013)
17. Liu, W., Cui, J., Xin, J.: A block-centered finite difference method for an unsteady asymptotic coupled model in fractured media aquifer system. J. Comput. Appl. Math. **337**, 319–340 (2018)
18. Lesinigo, M., D'Angelo, C., Quarteroni, A.: A multiscale Darcy–Brinkman model for fluid flow in fractured porous media. Numer. Math. **117**(4), 717–752 (2011)
19. Ahmed, R., Edwards, M.G., Lamine, S., Huisman, B.A.H., Pal, M.: Control-volume distributed multi-point flux approximation coupled with a lower-dimensional fracture model. J. Comput. Phys. **284**, 462–489 (2015)
20. Ahmed, R., Edwards, M.G., Lamine, S., Huisman, B.A.H., Pal, M.: Three-dimensional control-volume distributed multi-point flux approximation coupled with a lower-dimensional surface fracture model. J. Comput. Phys. **303**, 470–497 (2015)
21. Frih, N., Roberts, J.E., Saada, A.: Modeling fractures as interfaces: a model for Forchheimer fractures. Comput. Geosci. **12**(1), 91–104 (2008)
22. Knabner, P., Roberts, J.E.: Mathematical analysis of a discrete fracture model coupling Darcy flow in the matrix with Darcy–Forchheimer flow in the fracture. ESAIM: Math. Modell. Numer. Anal. **48**(5), 1451–1472 (2014)
23. Liu, W., Cui, J.: A two-grid block-centered finite difference algorithm for nonlinear compressible Darcy–Forchheimer model in porous media. J. Sci. Comput. **74**, 1786–1815 (2018)
24. Li, X., Rui, H.: A two-grid block-centered finite difference method for the nonlinear time-fractional parabolic equation. J. Sci. Comput. **72**, 863–891 (2017)
25. Rui, H., Pan, H.: A block-centered finite difference method for the Darcy-Forchheimer model. SIAM J. Numer. Anal. **50**(5), 2612–2631 (2012)
26. Rui, H., Liu, W.: A two-grid block-centered finite difference method for Darcy-Forchheimer flow in porous media. SIAM J. Numer. Anal. **53**(4), 1941–1962 (2015)
27. Weiser, A., Wheeler, M.: On convergence of block-centered finite differences for elliptic problems. SIAM J. Numer. Anal. **25**(2), 351–375 (1988)
28. Wheeler, M., Xue, G., Yotov, I.: A multipoint flux mixed finite element method on distorted quadrilaterals and hexahedra. Numer. Math. **121**(1), 165–204 (2012)
29. Wheeler, M., Yotov, I.: A multipoint flux mixed finite element method. SIAM J. Numer. Anal. **44**(5), 2082–2106 (2006)
30. Brenner, K., Hennicker, J., Masson, R., Samier, P.: Hybrid-dimensional modelling of two-phase flow through fractured porous media with enhanced matrix fracture transmission conditions. J. Comput. Phys. **357**, 100–124 (2017)
31. Ahmed, E., Jaffré, J., Roberts, J.E.: A reduced fracture model for two-phase flow with different rock types. Mathematics and Computers in Simulation, https://doi.org/10.1016/j.matcom.2016.10.005

Publisher's note Springer Nature remains neutral with regard to jurisdictional claims in published maps and institutional affiliations.